Supramolecular aggregation properties of 4-(1-morpholino)-1,8-naphthalimide based fluorescent materials

Supporting Information

June I. Lovitt,[a,d] Tumpa Gorai,[a] Emanuele Cappello,[a] Jason M. Delente,[a] Sebastian T. Barwich,[c] Matthias E. Mobius,[c] Thorfinnur Gunnlaugsson[a,d,e]*and Chris S. Hawes[b]**

[a] School of Chemistry and Trinity Biomedical Science Institute, University of Dublin, Trinity College Dublin, Dublin 2 (Ireland)

[b] School of Chemical and Physical Sciences, Keele University, Keele ST5 5BG, United Kingdom

[c]. School of Physics, Trinity College Dublin, The University of Dublin, Dublin 2, Ireland.

[d]. AMBER (Advanced Materials and Bioengineering Research) Centre, Trinity College Dublin, The University of Dublin, Dublin 2, Ireland.

[e]. Synthesis and Solid-State Pharmaceutical Centre (SSPC), Ireland.

Experimental

Materials and Methods

All reagents and solvents were used as received from Sigma-Aldrich, Merck or Fisher Scientific, were reagent grade or better and used without further purification. All NMR spectra were recorded using a Bruker Spectrospin DPX-400 instrument operating at 400 MHz for ^{1}H and 101 MHz for ^{13}C NMR or a Bruker AV-600 instrument operating at 600.1 MHz for 1H NMR and 150.9 MHz for ^{13}C NMR. Chemical shifts are reported in ppm with the residual solvent as the internal reference. All NMR spectra were carried out at 293 K. Melting points were determined using an Electrothermal IA9000 digital melting point apparatus in an unsealed capillary tube and are uncorrected. Infrared spectra were recorded on PerkinElmer Spectrum One FTIR spectrometer in the range 4000 - 650 cm^{-1}. Mass spectra were acquired using a Micromass time of flight mass spectrometer (tof), interfaced to a Waters 2690 HPLC. The instrument was operated in positive or negative mode as required. Masses was recorded over the range 100-1000 m/z. Thermogravimetric analysis of **L1**, **L2** and gels **1** and **2** were performed on Perkin Elmer Pyrus 1 TGA equipped with an ultra-micro balance with a sensitivity of 0.1 microgram. The temperature range is from 25 - 500 °C with a scan rate 5 °C min^{-1}, under a N2 purge flow of 20 $mL.min^{-1}$. Scanning Electron Microscopy was carried out on Carl Zeiss Ultra SEM. The samples were coated with a thin layer of gold using a sputtering procedure. Phase purity of all crystalline materials was confirmed with X-ray powder diffraction patterns recorded with a Bruker D2 Phaser instrument using Cu-Kα (λ = 1.5405 Å) radiation. Samples were finely ground and applied to a quartz sample holder. Raw data were compared with the simulated patterns from the single crystal data collections carried out at 100 K. All measurements were carried out in duplicate to ensure reproducibility. Elemental analysis was carried out on Exeter Analytical CE440 elemental analyser at the microanalysis laboratory, School of Chemistry and Chemical Biology, University College Dublin. Rheological measurements were carried out with an Anton Paar MCR 301 rheometer using a plate-plate geometry with a sandblasted plate to prevent slip. The diameter of the plates was 50mm and the gap size was set to 0.5mm. All measurements were performed at 20°C using a solvent trap to minimise evaporation during the measurement. After loading the gels into the rheometer, all samples were allowed to rest for 30 minutes prior to measurement. All measurements were carried out in duplicate to ensure reproducibility.

X-ray Crystallography

Diffraction data were collected using a Bruker APEX-II Duo dual-source instrument using graphite-monochromated Mo Kα (λ = 0.71073 Å) or microfocus Cu Kα (1.5405 Å) radiation as specified. Datasets were collected using ω and ϕ scans with the samples immersed in oil and maintained at a constant temperature of 100 K using a Cobra cryostream. The reflection data were reduced and processed using the Bruker APEX-3 suite of programs.[S1] Multi-scan absorption corrections were applied using SADABS.[2] The diffraction data were solved using direct methods with SHELXT and refined by full matrix least-squares procedures with SHELXL-2015 within the OLEX-2 GUI.[S3-S5] All non-hydrogen atoms were refined with anisotropic displacement parameters. All carbon-bound hydrogen atoms were placed in calculated positions and refined with a riding model, with isotropic displacement parameters equal to either 1.2 or 1.5 times the isotropic equivalent of their carrier atoms. Where appropriate, the positions of the hydrogen atoms involved in hydrogen bonding interactions were refined to provide the best fit for the residual Fourier peaks and assigned a U_{iso} value equal to 1.5 times that of the nearest associated atom, with the appreciation that the exact positions of these atoms cannot be meaningfully inferred from X-ray diffraction data. Specific refinement strategies are outlined in the combined crystallographic information file. CCDC 2048284-2048287.

Photophysical Measurements

Unless otherwise stated, all measurements were performed at 298 K in Millipore filtered deionised water. UV-Vis absorption spectra were measured in 10 mm path length, 3 mL quartz cuvettes (Hellma) on a Varian Cary 50 spectrophotometer in the range 230-800 nm (CH_3CN) or 250–800 nm ($CHCl_3$). Baseline correction was applied for all spectra. Fluorescence spectra was measured on a Varian Cary Eclipse fluorimeter. pH values of the solutions were recorded with a calibrated 827 Metrohm laboratory pH meter. NaCl (100 mM) was used as an ionic medium. Solid state fluorescence emission spectra were measured on a Spectramax Gemini XS Dual-Scanning Microplate Spectrofluorometer.

Synthesis and Characterisation

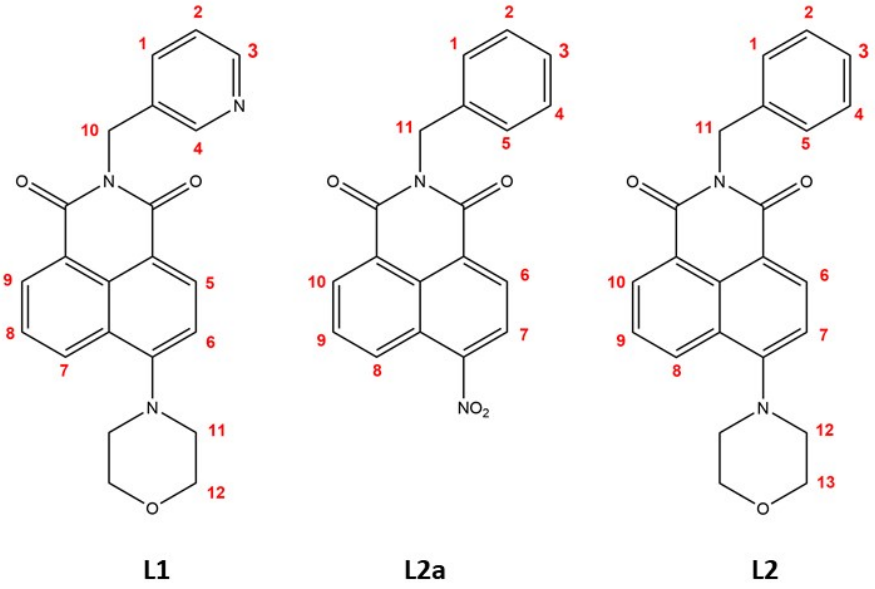

Fig. S1: *Structures and ^{1}H NMR labelling schemes for ligands **L1**, **L2a** and **L2**.*

***N*-(3-picolyl)-4-(1-morpholino)-1,8-naphthalimide (L1)**

The synthesis of **L1** was carried out according to a modified literature procedure.[S6] *N*-(3-picolyl)-4-nitro-1,8-napthalimide (150 mg, 0.52 mmol, 1 eq) and morpholine (0.140 mL, 1.56 mmol, 3 eq) was refluxed under nitrogen in DMF for 4 hours at 140°C. The reaction mixture was cooled, poured into CH_2Cl_2 (100 mL) and subsequently washed twice with H_2O. The organic phase was filtered through $MgSO_4$ and evaporated to dryness yielding a yellow powder. Yield (109 mg, 65%) m.p. 170-172 °C Found C 69.64 H 5.22 N 11.08 Anal. Calc. for $C_{22}H_{19}N_3O_{3.0}\cdot 0.33H_2O$ C 69.68 H 5.23 N 11.09% δ_H (400 MHz, d_6- DMSO) δ 8.61(s, 1H, H^4), 8.50(dd, $^3J_1$ = 7.8 Hz, $^3J_2$ = 4.8 Hz, 2H, H^6 + H^7), 8.43 (d, ^3J = 7.3Hz, 2H, H^5 +H^8), 7.81(t, ^3J=7.9Hz, 1H, H^3), 7.72 (d, ^3J=7.7 Hz, 1H, H^9), 7.36 (d, ^3J=8.1 Hz, 1H, H^1), 7.30 (dd, $^3J_1$ = 7.8 Hz, $^3J_2$ = 4.8 Hz, 1H, H^2), 5.24 (s, 2H, H^{10}), 3.89 (s, 4H, H^{12}), 3.22 (s, 4H, H^{11}). δ_C (101 MHz, $CDCl_3$,) δ 163.70, 163.14, 155.77, 149.22, 148.30, 135.40, 133.18, 132.54, 131.00, 130.91, 129.31, 126.17, 125.31, 123.54, 122.47, 115.62, 115.15, 66.16, 53.03, 40.49, 30.94, 22.05. IR ν_{max} (cm^{-1}): 2916w, 1692s, 1647s, 1573s, 1556s, 1509w, 1455w, 1427w, 1376s, 1344s, 1315s, 1315s, 1230s, 1173m, 1119m, 1030m, 1026m, 973m, 936m, 830m, 780s, 710s, 707s, 622m. HRMS (m/z) Calculated for $C_{22}H_{20}N_3O_3$ *m/z* = 374.1460. Found for $[M+H]^+$ *m/z* = 374.1494. UV-vis (CH_3OH) λ_{max}/nm ($\times 10^3$ ε_{max}/L·mol^{-1}·cm^{-1}): 255 (16.6 ± 0.2), 400 (11.1±0.1).

***N*-(benzyl)-4-nitro-1,8-naphthalimide (L2a)**

The synthesis of **L2a** was carried out according to literature procedures.[S6] To a suspension of 4-nitro-1,8-naphthalic anhydride (500 mg, 2.06 mmol, 1 eq) and AcOH (8 mL), benzylamine (0.45 mL, 4.11 mmol, 2 eq) was added and the mixture was heated under reflux for six hours. After cooling to room temperature, the reaction mixture was poured into H_2O (100 mL), which produced a yellow precipitate. The mixture was then taken to pH 6 with aqueous KOH to aid precipitation. The resulting precipitate was filtered and washed with MeOH and Et_2O and dried in air. Yield (300mg, 90%) m.p. 157-158 °C Found C 68.22 H 3.37 N 8.24 Anal. Calc. for $C_{19}H_{12}N_2O_4$ C 68.67 H 3.64 N 8.43. δ_H (600 MHz, $CDCl_3$) δ 8.84 (d, ^3J = 8.5 Hz, 1H, H^6), 8.75 (d, ^3J = 7.3 Hz, 1H, H^5), 8.70 (d, ^3J = 8.0 Hz, 1H, H^8), 8.40 (d, ^3J = 8.0 Hz, 1H, H^4), 7.98 (dd, $^3J_1$ = 8.6 Hz , $^3J_2$ = 7.5 Hz, 1H, H^7), 7.54 (d, ^3J = 7.4 Hz, 2H, H^2), 7.32 (t, ^3J = 7.5 Hz, 2H, H^3), 7.27 – 7.25 (m, 2H, H^1), 5.38 (s, 2H, H^9). δ_C (101 MHz, $CDCl_3$) δ 163.36, 162.54, 149.69, 136.60, 132.70, 130.05, 129.97, 129.48, 129.16, 129.09, 128.59, 127.83, 126.98, 123.91, 123.72, 123.33, 123.01, 43.96, 30.95. IR ν_{max} (cm^{-1}): 3080w, 1702s, 1655s, 1583m, 1529s, 1380s, 1331s, 1229s, 1179s, 1070m, 824m, 784s, 756s, 699s, 665m. HRMS (*m/z*) Calculated for $C_{19}H_{12}N_2O_4$ *m/z* = 332.0797 Found for $[M+H]^+$ *m/z* =332.0803. UV-vis (CH_3OH) λ_{max}/nm ($\times 10^3$ ε_{max}/L·mol^{-1}·cm^{-1}): 232 (12.6± 0.2), 348 (4.8±0.08).

_N_-(benzyl)-4-(1-morpholino)-1,8-naphthalimide (L2)

The synthesis of **L2** was carried out according to a modified literature procedure.[S6] *N*-(benzyl)-4-nitro-1,8-napthalimide (100 mg, 0.3 mmol, 1 eq) and morpholine (0.08 mL, 0.9 mmol, 3 eq) was refluxed in DMF for 4 hours at 140°C. The reaction mixture was cooled, poured into CH_2Cl_2 (100 mL) and subsequently washed twice with H_2O. The organic phase was filtered through $MgSO_4$ and evaporated to dryness yielding a yellow powder. Yield (90 mg, 53%) m.p. 168-170 °C. Found C 73.39 H 4.97 N 7.25 Anal. Calc. for $C_{23}H_{20}N_2O_3 \cdot 0.1H_2O$ C 73.82 H 5.44 N 7.49. δ_H (600 MHz, $CDCl_3$) δ 8.63 (d, ^3J = 7.2 Hz, 1H, H^6), 8.57 (d, ^3J = 8.1 Hz, 1H, H^8), 8.44 (d, ^3J = 8.4 Hz, 1H, H^4), 7.75– 7.69 (m, 2H, H^5 +H^7), 7.55 (d, ^3J = 7.6 Hz, 2H, H^2), 7.32 (d, ^3J = 7.5 Hz, 2H, H^3), 7.26 (d, ^3J = 8.0 Hz, 2H, H^1), 5.39(s, 2H, H^9), 4.04 (s, 4H, H^{11}), 3.28 (s, 4H, H^{10}). δ_C (101 MHz, $CDCl_3$,) δ 164.46, 164.00, 155.76, 137.48, 132.78, 131.42, 130.20, 129.96, 128.87, 128.41, 127.38, 126.16, 125.87, 123.32, 117.13, 115.00, 66.97, 53.45, 30.94. ν_{max} (cm^{-1}): 2858w, 1648s, 1583s, 1529s, 1380m, 1349s, 1331s, 1314s, 1232m, 1179m, 1113m, 825w, 782s, 756s, 699s. HRMS (*m/z*) Calculated for $C_{23}H_{21}N_2O_3$ *m/z* = 373.1552. Found for $[M+H]^+$ *m/z* =374.15467. UV-vis (CH_3OH) λ_{max}/nm (×10^3 ε_{max}/L·mol^{-1}·cm^{-1}): 255 (49.8± 0.2), 397 (4.8±0.08).

L1-Mn gel 1

Ligand **L1** (10 mg, 27 µmol, 1 eq) was dissolved in MeCN (1.25mL) at room temperature affording a yellow solution (sol I). $MnCl_2 \cdot 4H_2O$ (5 mg, 30 µmol, 1 eq) was suspended in MeCN (1.25 mL) at room temperature with the aid of sonication affording a yellow suspension (sol II). Sol II was added rapidly at room temperature to sol I and the resulting mixture was gently heated to 50°C to form a homogenous solution. When left to stand overnight this solution formed a yellow homogenous gel.

L1-Co gel 2

Ligand **L1** (10 mg, 27 µmol, 1 eq) was dissolved in MeCN (1.25mL) at room temperature affording a yellow solution (sol I). $CoCl_2 \cdot 6H_2O$ (6 mg, 27 µmol, 1 eq) was suspended in MeCN (2.5 mL) at room temperature with the aid of sonication affording a blue solution (sol II). Sol II was added rapidly at room temperature to sol I and the resulting mixture was gently heated to 50°C to form a homogenous solution. When left to stand overnight this solution formed a green homogenous gel.

L1-Ni gel 3

Ligand **L1** (20 mg, 54 µmol, 1 eq) was dissolved in MeCN (2.5mL) at room temperature affording a yellow solution (sol I). $NiCl_2 \cdot 6H_2O$ (13 mg, 54 µmol, 1 eq) was suspended in MeCN (2.5 mL) at room temperature with the aid of sonication affording a blue solution (sol II). Sol II was added rapidly at room temperature to sol I and the resulting mixture was gently heated to 50°C to form a homogenous solution. When left to stand overnight this solution formed a weak, green gel.

Table S1: Crystallographic and Refinement Parameters for All Structures

Identification code	**L1**	**L1-gel**	**L2a**	**L2**
Empirical formula	$C_{22}H_{27}N_3O_7$	$C_{20}H_{20}N_2O_2$	$C_{23}H_{20}N_2O_3$	$C_{19}H_{12}N_2O_4$
Formula weight	445.46	320.38	372.41	332.31
Temperature/K	100.0	100.0	100.0	100.0
Crystal system	monoclinic	monoclinic	monoclinic	orthorhombic
Space group	$P2_1$	$P2_1/c$	$P2_1/c$	*Pbca*
a/Å	4.4753(3)	4.7218(5)	15.4559(16)	6.9839(7)
b/Å	14.6485(8)	11.9820(11)	7.0602(7)	17.9787(19)
c/Å	16.3368(9)	30.536(3)	17.1898(17)	23.148(2)
α/°	90	90	90	90
β/°	90.416(4)	92.951(7)	111.632(3)	90
γ/°	90	90	90	90
Volume/Å^3	1070.95(11)	1725.3(3)	1743.7(3)	2906.5(5)
Z	2	4	4	8
ρ_{calc}g/cm^3	1.381	1.233	1.419	1.519
μ/mm^{-1}	0.867	0.641	0.095	0.109
F(000)	472.0	680.0	784.0	1376.0
Crystal size/mm^3	0.07 × 0.05 × 0.05	0.08 × 0.03 × 0.03	0.16 × 0.05 × 0.05	0.427 × 0.077 × 0.046
Radiation	CuKα (λ = 1.54178)	CuKα (λ = 1.54178)	MoKα (λ = 0.71073)	Mo Kα (λ = 0.71073)
2Θ range for data collection/°	5.41 to 138.88	5.796 to 108.612	5.67 to 55.132	4.862 to 52.852
Index ranges	-4 ≤ h ≤ 4, -15 ≤ k ≤ 15, -17 ≤ l ≤ 17	-4 ≤ h ≤ 4, -12 ≤ k ≤ 12, -32 ≤ l ≤ 31	-20 ≤ h ≤ 19, -9 ≤ k ≤ 9, -22 ≤ l ≤ 22	-8 ≤ h ≤ 8, -22 ≤ k ≤ 22, -28 ≤ l ≤ 28
Reflections collected	10624	11302	24037	36980
Independent reflections	2791 [R_{int} = 0.0578, R_{sigma} = 0.0470]	2094 [R_{int} = 0.1082, R_{sigma} = 0.1205]	4016 [R_{int} = 0.0791, R_{sigma} = 0.0499]	2990 [R_{int} = 0.2123, R_{sigma} = 0.0776]
Data/restraints/parameters	2791/1/309	2094/0/253	4016/0/325	2990/0/226
Goodness-of-fit on F^2	1.043	1.075	1.016	1.054
Final R indexes [I>=2σ (I)]	R_1 = 0.0386, wR_2 = 0.0959	R_1 = 0.0749, wR_2 = 0.1824	R_1 = 0.0494, wR_2 = 0.1058	R_1 = 0.0827, wR_2 = 0.1733
Final R indexes [all data]	R_1 = 0.0429, wR_2 = 0.0987	R_1 = 0.1159, wR_2 = 0.2058	R_1 = 0.0888, wR_2 = 0.1236	R_1 = 0.1678, wR_2 = 0.2147
Largest diff. peak/hole / e Å^{-3}	0.16/-0.17	0.24/-0.25	0.27/-0.26	0.41/-0.31
Flack parameter	-0.03(16)	n/a	n/a	n/a

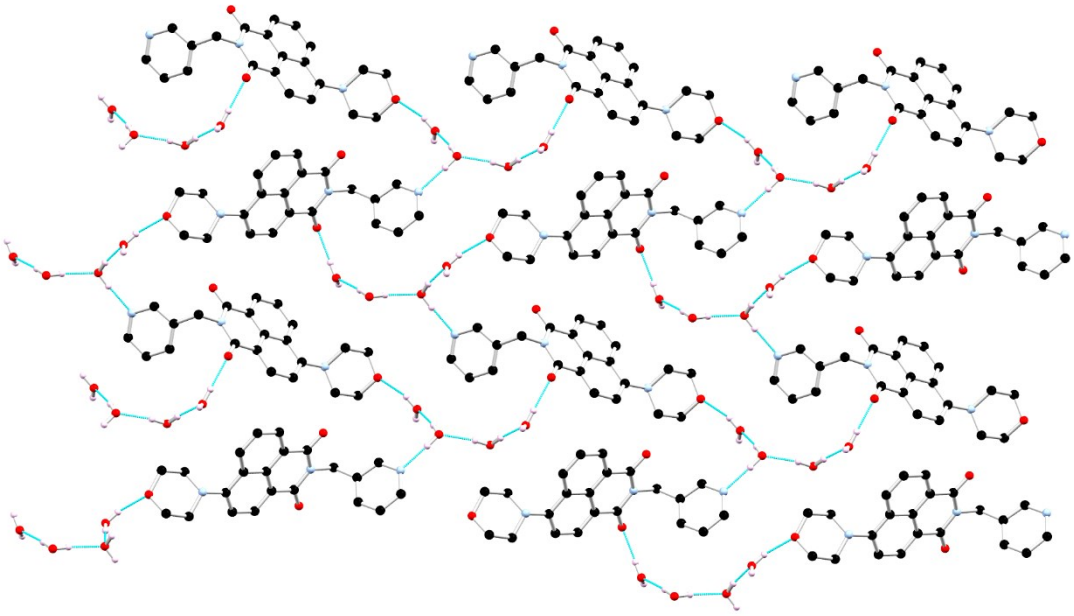

Fig. S2*: Extended structure of* ***L1*** *featuring hydrogen bonding and π···π stacking interactions between adjacent ligand moieties. Hydrogen atoms not involved in hydrogen bonding are omitted for clarity.*

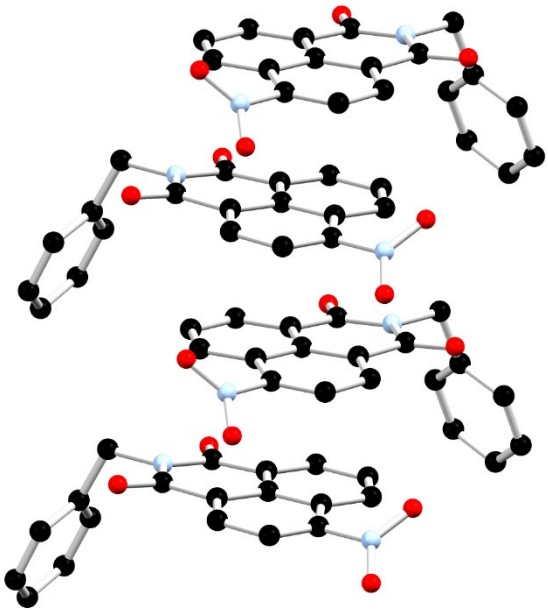

Fig. S3*: Extended structure of* ***L2a*** *featuring offset head-to-tail π···π stacking interactions between adjacent naphthalimide rings. Hydrogen atoms are omitted for clarity.*

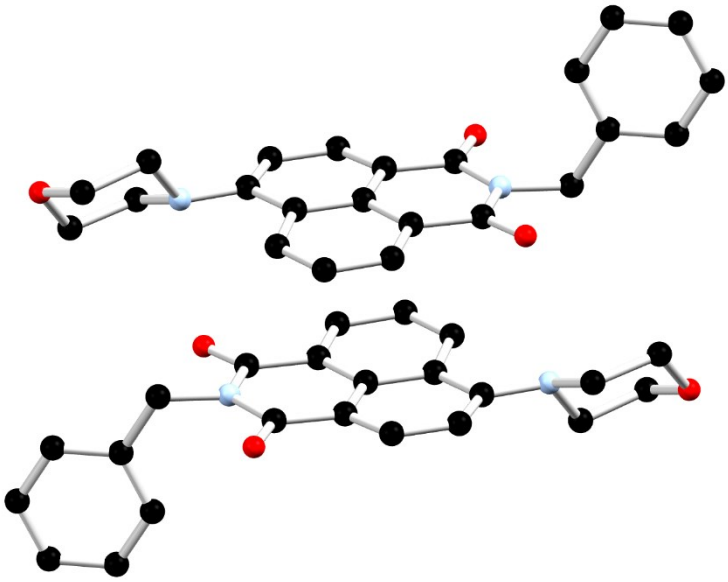

Fig. S4*: Extended structure of **L2** featuring offset head-to-tail π···π stacking interactions between adjacent naphthalimide rings. Hydrogen atoms are omitted for clarity.*

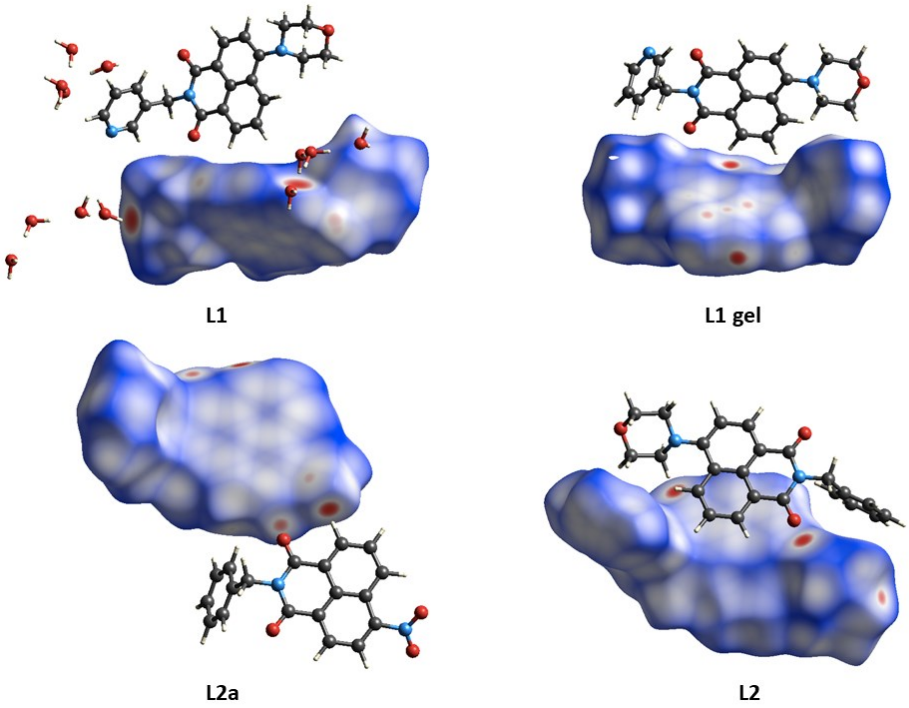

Fig. S5: *Calculated Hirshfeld (d_{norm}) surface with normalised contact distance (D_{norm}) mapping for **L1**, **L1-gel**, **L2a** and **L2** showing the main C-H···O interactions for each compound. Figures prepared with CrystalExplorer software, rendered with surface property in the range -0.65 to +1.35.* [S7-8]

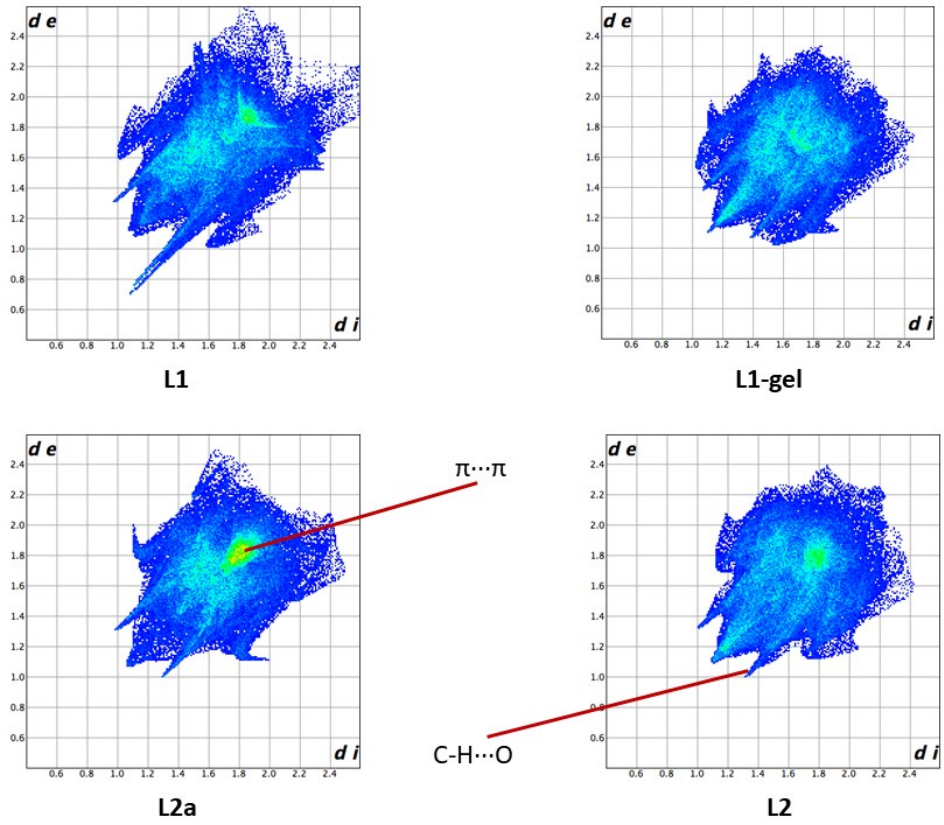

Fig. S6: *Calculated Fingerprint plots from Hirshfeld surface for **L1**, **L1-gel**, **L2a** and **L2** showing the main C-H···O interactions for each compound.*

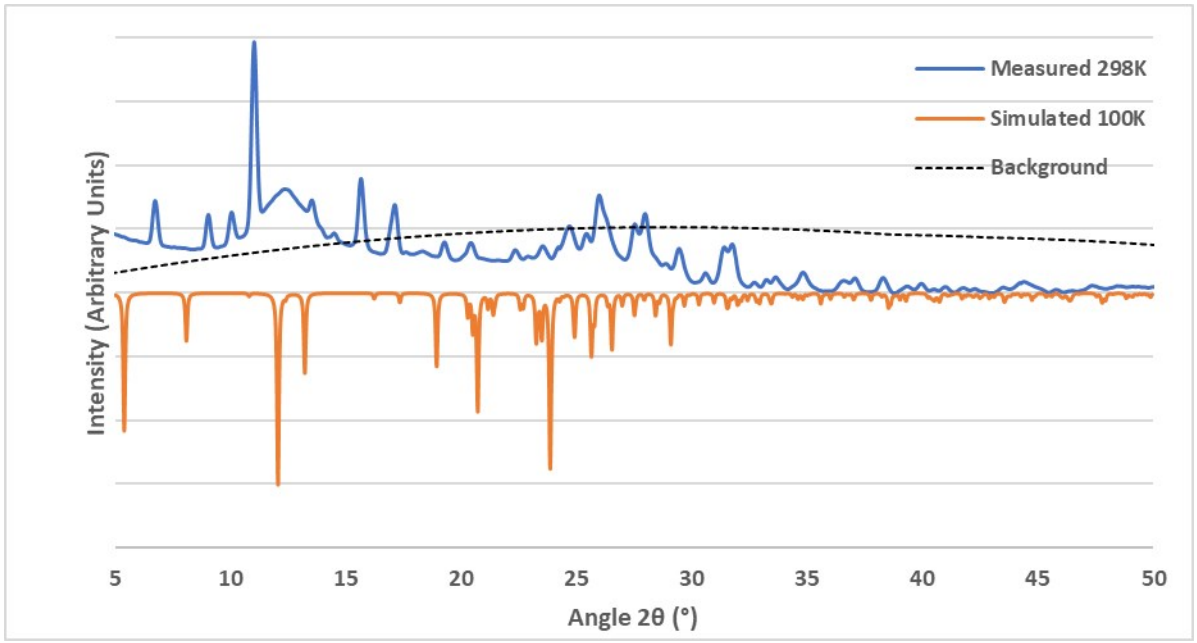

Fig. S7*: X-ray powder diffraction pattern for **L1** collected at 298 K compared to the calculated pattern from the single crystal dataset at 100 K.*

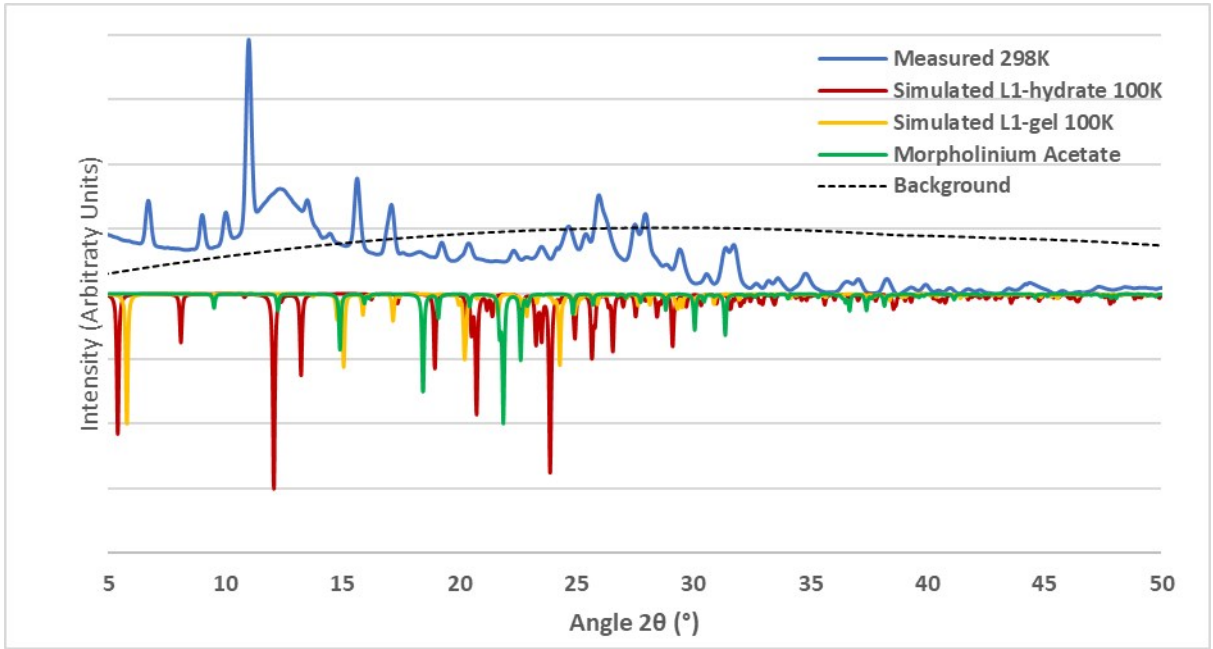

Fig. S8*: X-ray powder diffraction pattern for **L1** collected at 298 K compared to the calculated patterns from the single crystal datasets for **L1** and **L1-gel** at 100 K and the calculated pattern from morpholinium acetate (CCDC 918420).*[S9]

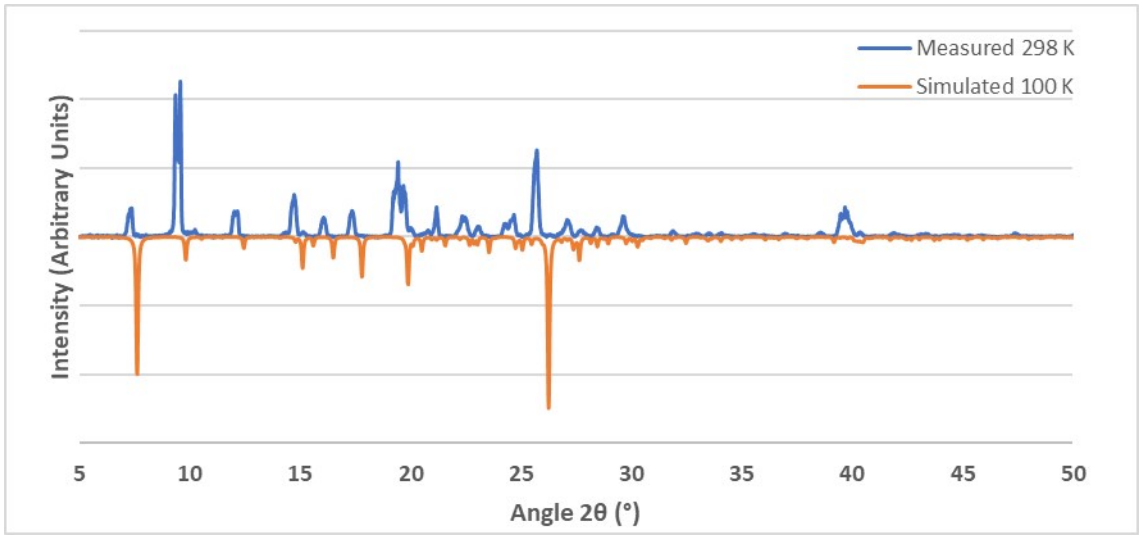

Fig. S9: *X-ray powder diffraction pattern for **L2a** collected at 298 K compared to the calculated pattern from the single crystal dataset at 100 K.*

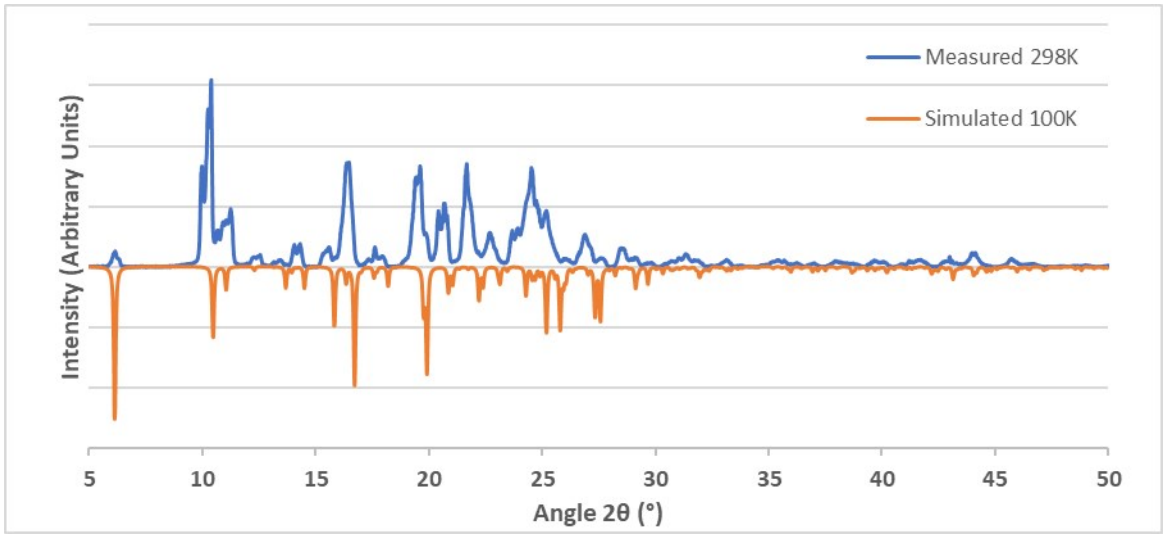

Fig. S10 *: X-ray powder diffraction pattern for **L2** collected at 298 K compared to the calculated pattern from the single crystal dataset at 100 K.*

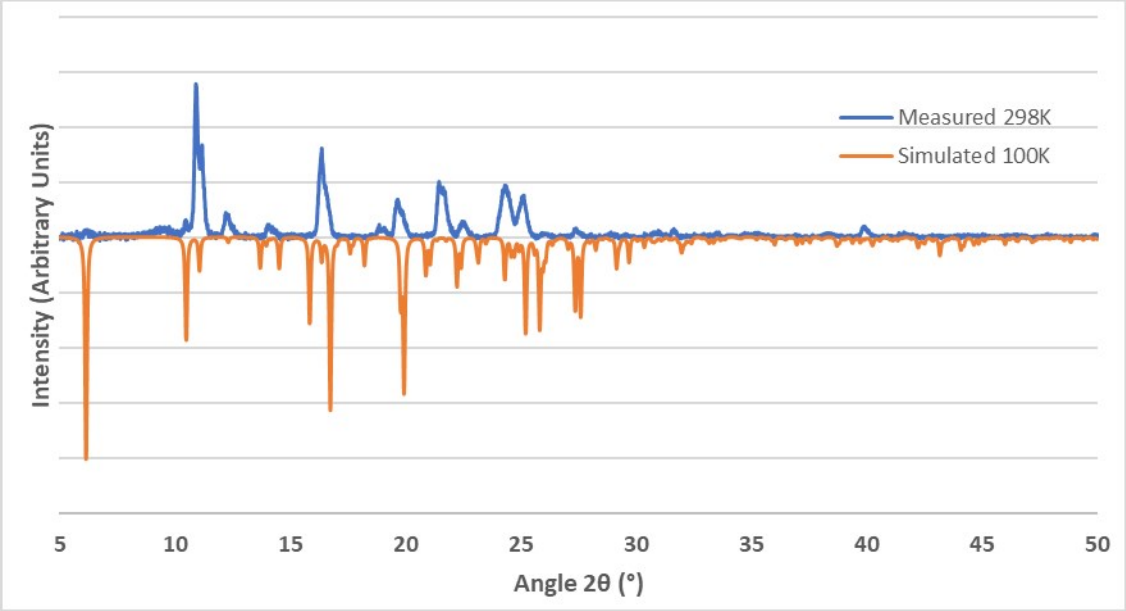

Fig. S11: *X-ray powder diffraction pattern for **L2-Mn** collected at 298 K compared to the calculated pattern from the single crystal dataset for **L2**, measured at 100 K.*

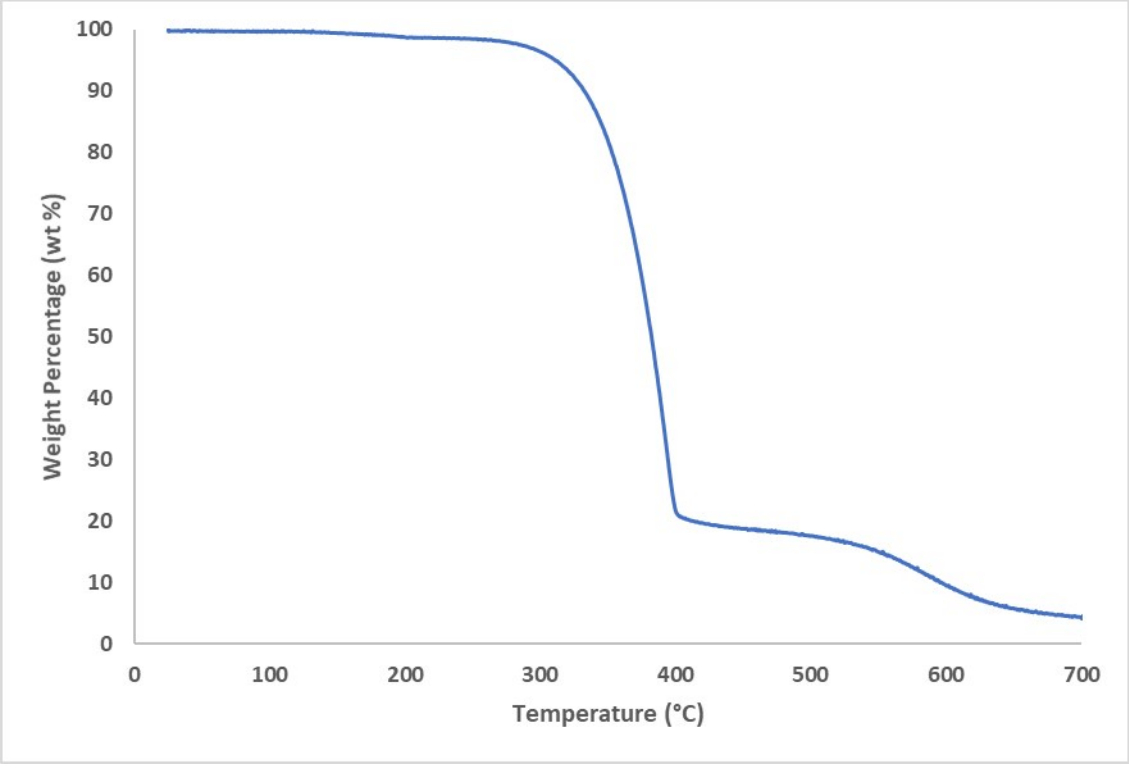

Fig. S12: *Thermogravimetric analysis of **L1***.

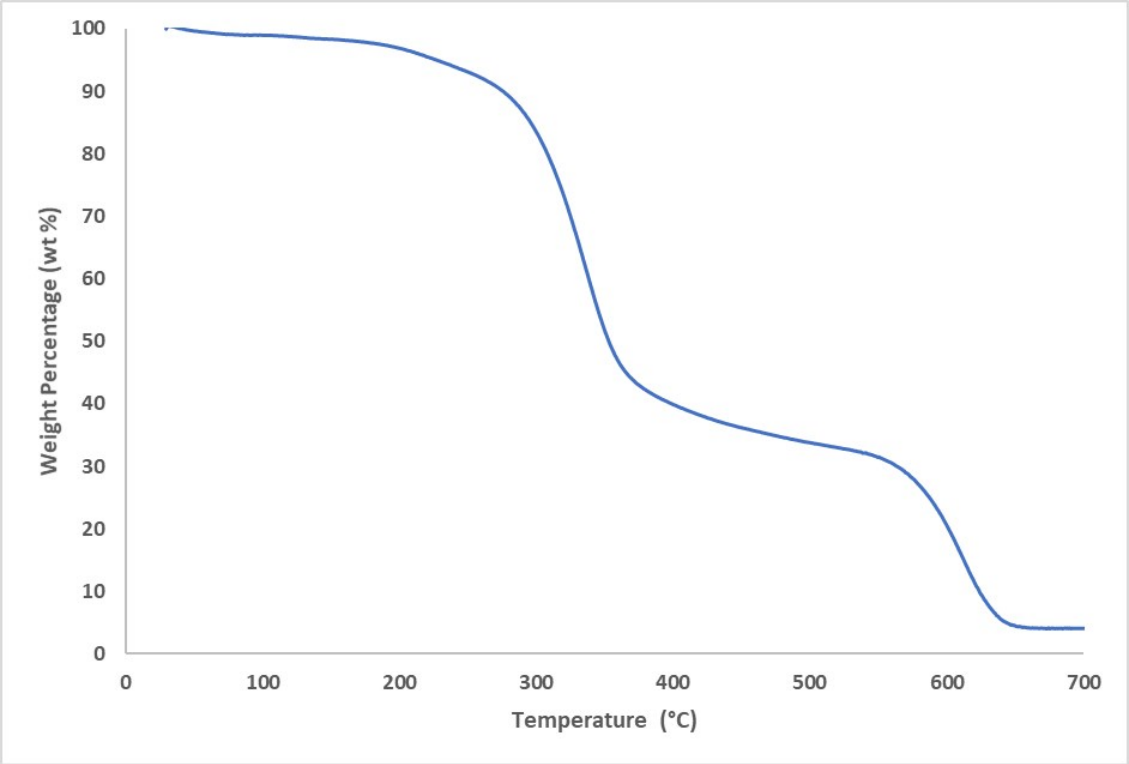

Fig. S13: *Thermogravimetric analysis of **L2***.

Photophysical Properties

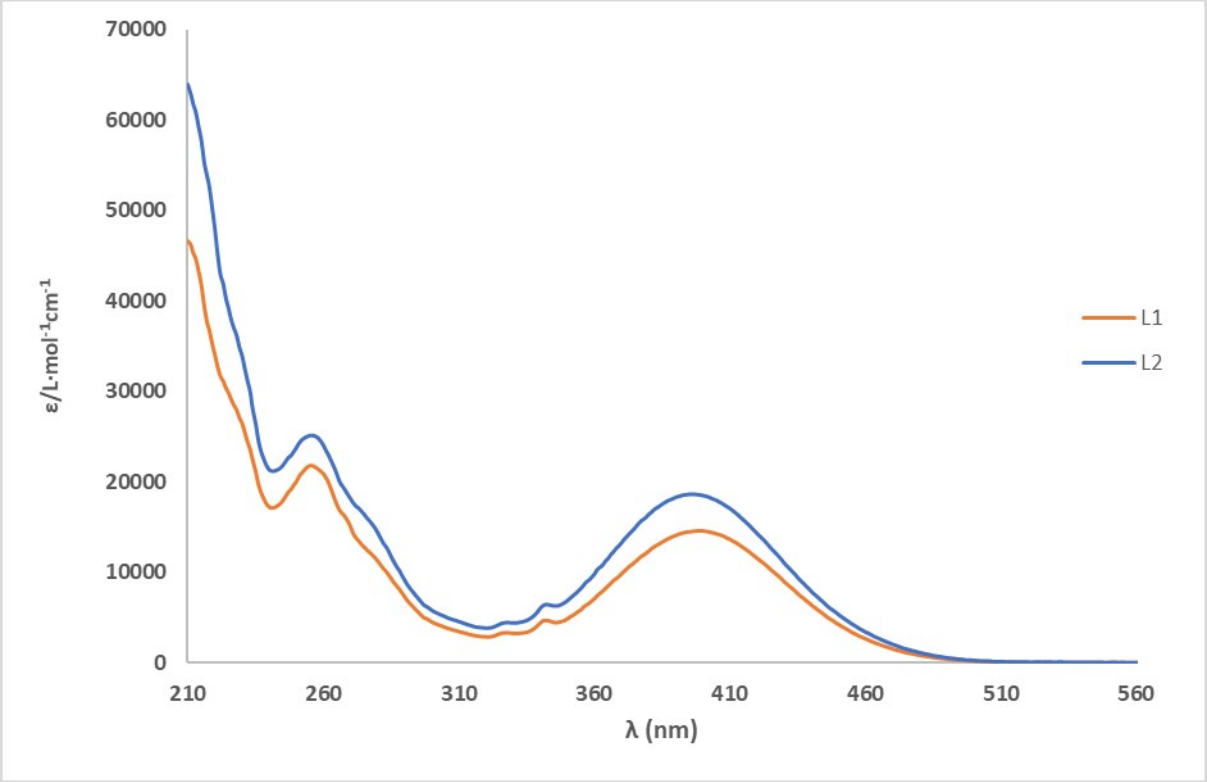

Fig. S14: *UV absorption spectra of **L1** and **L2** (CH_3OH) at $2x10^{-5}$M concentration.*

Solvatochromism

Table **S2**: *Photophysical parameters of **L1***.

Solvent	Dielectric constant (ε)[S10]	Refractive index (n)[S10]	Absorption maxima (nm)	Absorption maxima (cm^{-1})	Fluorescence emission maxima (nm)	Fluorescence emission maxima (cm^{-1})	Stokes shift (cm^{-1})
Methanol	32.7	1.46	396	25300	539	18600	6700
Acetonitrile	37.5	1.34	395	25300	530	18900	6400
THF	7.58	1.41	391	25600	514	19500	6100
DCM	8.93	1.42	392	25500	511	19600	5900
Toluene	2.38	1.49	392	25500	515	19400	6100
DMSO	46.7	1.48	402	24900	542	18400	6500

Solvent	Dielectric constant (ε)[S10]	Refractive Index (n)[S10]	Absorption maxima (nm)	Absorption maxima (cm^{-1})	Fluorescence emission maxima (nm)	Fluorescence emission maxima (cm^{-1})	Stokes shift (cm^{-1})
Methanol	32.7	1.46	398	25100	528	18900	6200
Acetonitrile	37.5	1.34	397	25200	530	18900	6300
THF	7.58	1.41	395	25300	516	19400	5900
DCM	8.93	1.42	398	25100	515	19400	5700
Toluene	2.38	1.49	398	25100	514	19400	5700
DMSO	46.7	1.48	406	24600	533	18800	5800

Table **S3**: Photophysical parameters of **L2**.

The Lippert-Mataga Equation

To examine the solvatochromism of the system, the difference between the excited and ground state dipole moment, Δμ, was calculated using the Lippert-Mataga equation [eqn. (1)]. In which $\Delta\nu = \nu_{abs} - \nu_{em}$ is the Stokes shift, ν_{abs} and ν_{em} are the absorption and emission frequency (cm^{-1}), ħ is Plank's constant, *c* is the speed of light in a vacuum, *a* is the effective radius of the Onsagar cavity of a compound. Δf is Lippert's solvent polarity, ε is the refractive index, *n* is the dielectric constant of each solvent. [S11]

Eqn. 1:

$$\Delta\nu = \nu_{abs} - \nu_{em} = \frac{2\Delta f}{\hbar c a^3}(\mu_E - \mu_G)^2 + constant$$

$$\Delta f = \frac{\varepsilon - 1}{2\varepsilon + 1} - \frac{n^2 - 1}{2n^2 + 1}$$

Therefore:

$$\nu_{abs} - \nu_{em} = \frac{2}{\hbar c}\left(\frac{\varepsilon - 1}{2\varepsilon + 1} - \frac{n^2 - 1}{2n^2 + 1}\right)\frac{(\mu_E - \mu_G)^2}{a^3} + constant$$

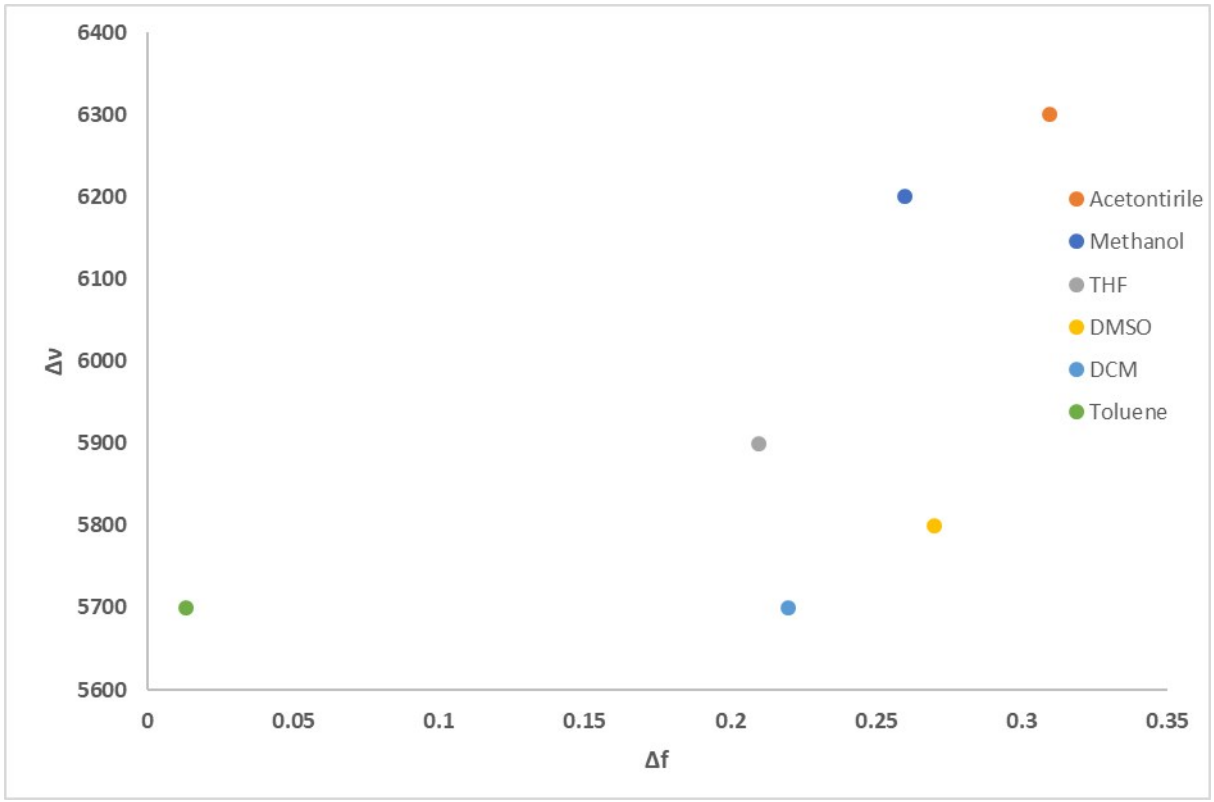

Fig. S15: *Lippert-Mataga plot of **L1***

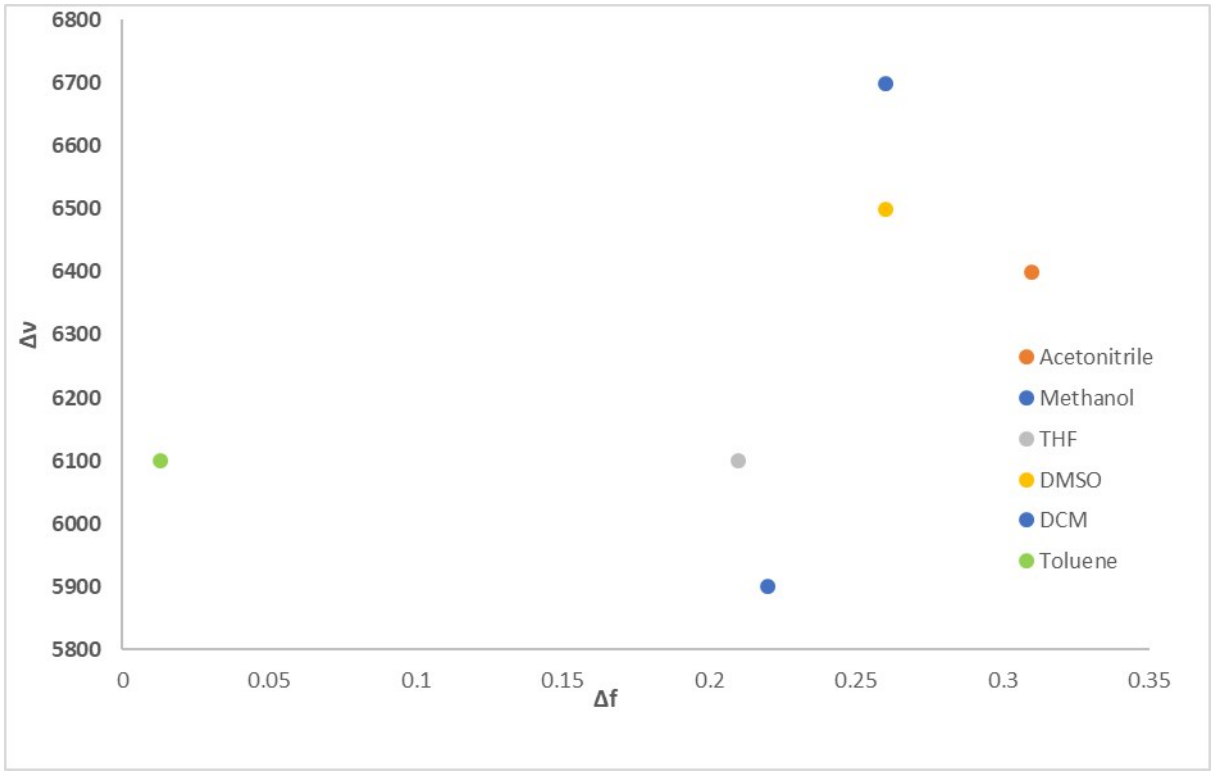

Fig. S16: *Lippert Mataga plot of **L2**.*

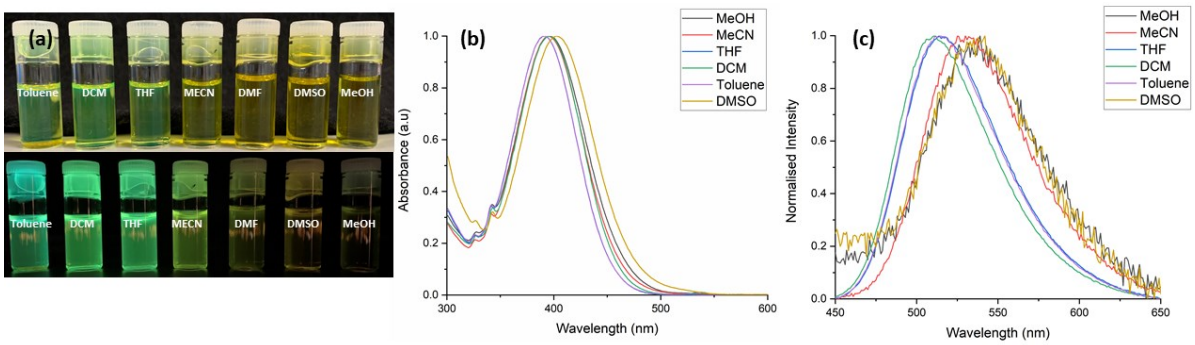

Fig. S17: *UV absorption spectra of **L2** in solvents of varying polarity, Fluorescence spectra of **L2** in solvents of varying polarity.*

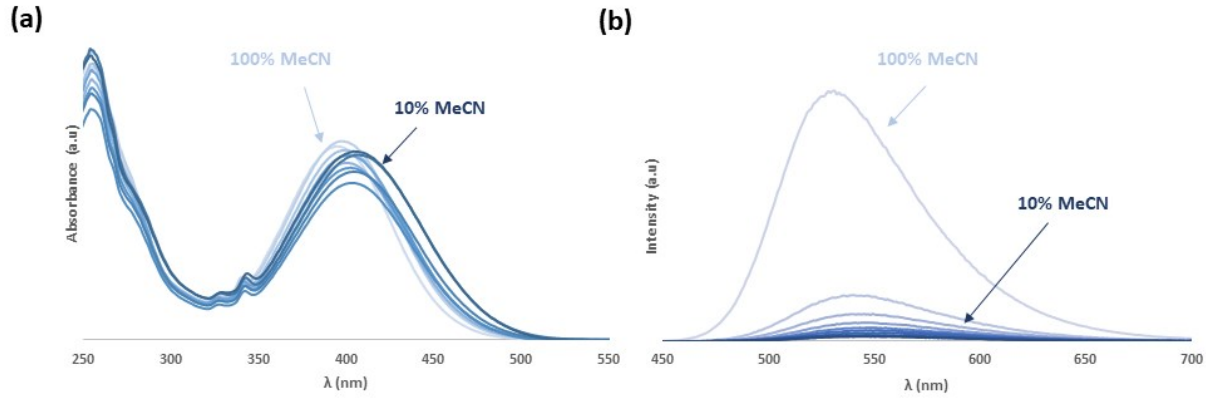

Fig S18: **(a)** UV-vis spectra of **L1** in *(1.5x10^{-5}M) in $CH_3CN – H_2O$ mixtures with various water contents (0-90 %).* (**b**) *Fluorescence Emission spectra (λ_{ex} = 400nm, λ_{max} = 530nm) of **L2** (1.5x10^{-5}M) in CH_3CN-H_2O mixtures with various water contents (0-90%).*

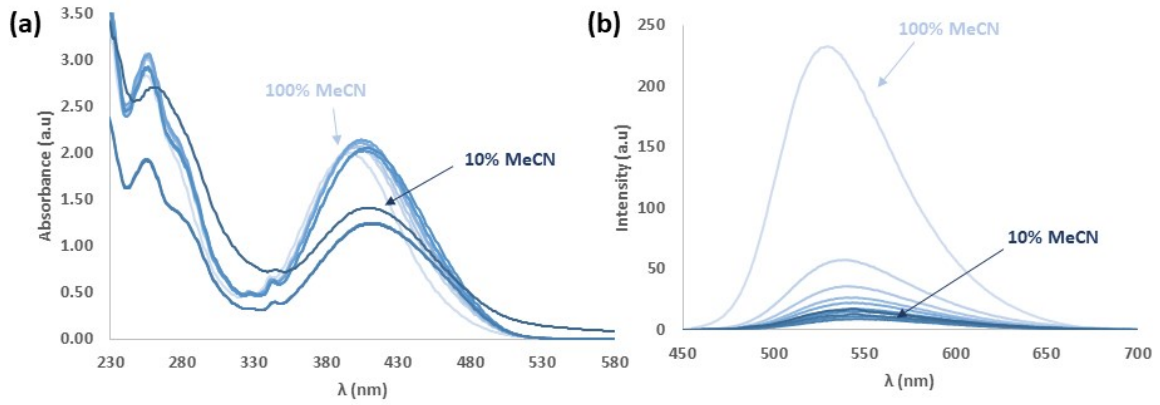

Fig. S19: (**a**) *UV-Vis spectra of **L2** (1.5x10^{-5}M) in $CH_3CN – H_2O$ mixtures with various water contents (0-90 %).* (**b**) *Fluorescence Emission spectra (λ_{ex} = 400nm, λ_{max} = 530nm) of **L2** (1.5x10^{-5}M) in CH_3CN-H_2O mixtures with various water contents (0-90%).*

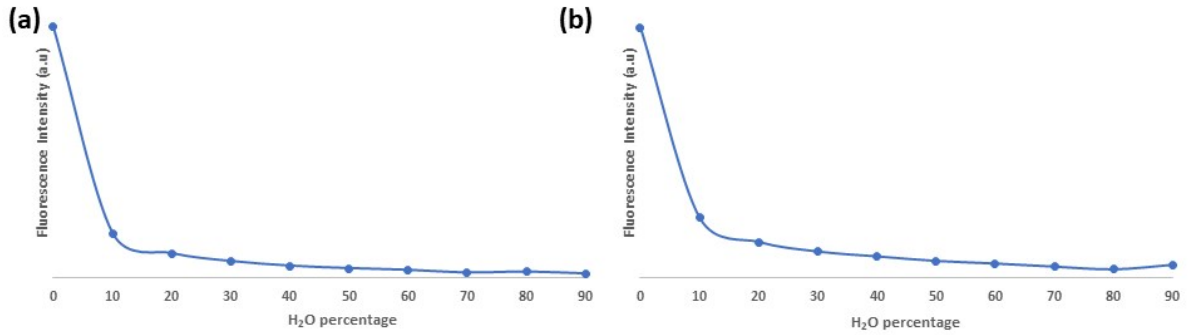

***Fig. S20**: (a) Fluorescence intensity as function of the percentage of H_2O fraction for **L1**. (b) Fluorescence intensity as a function of H_2O fraction for **L2**.*

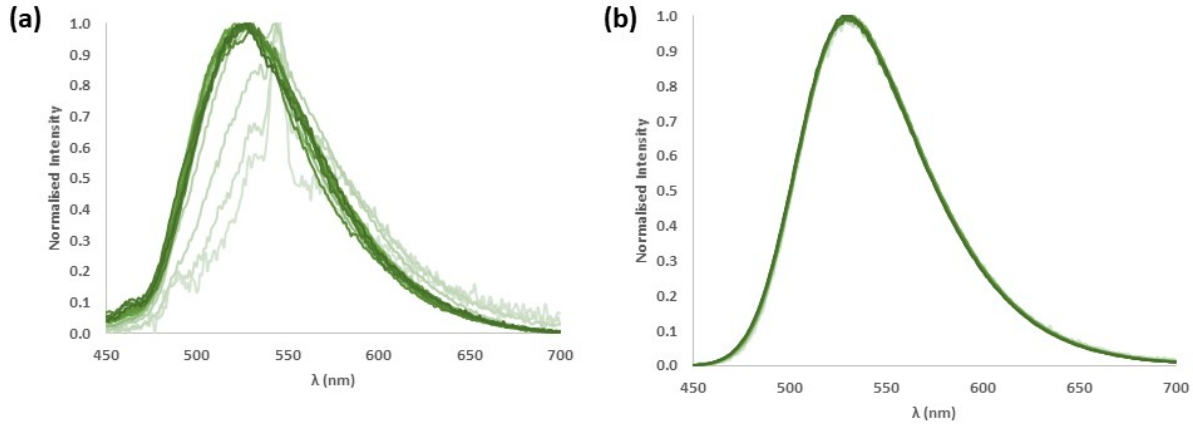

Fig. S21: ***(a)** Fluorescence emission spectra (λ_{ex} = 400nm, λ_{max} = 530nm) of the concentration dependent study of **L1** over the range (1×10^{-4}M to 1×10^{-6}M) recorded in H_2O. (**b**) Fluorescence emission spectra (λ_{ex} = 400nm, λ_{max} = 530nm) of **L1** over the concentration range (1×10^{-4}M to 1×10^{-6}M) recorded in CH_3CN. The sharp peak present in the lower concentration samples is a Raman scattering band from the solvent (Figure S23).*[S11]

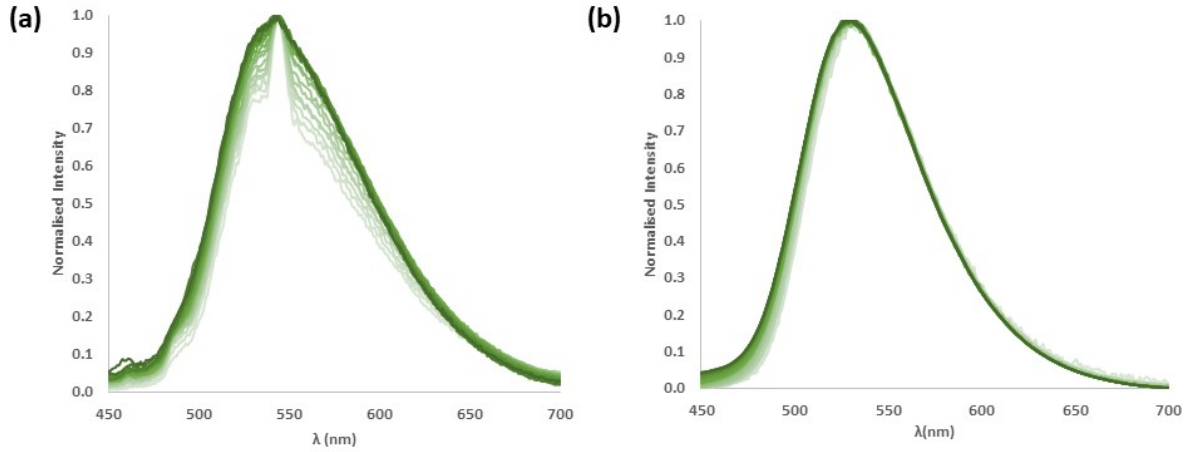

Fig. S22: ***(a)** Fluorescence emission spectra (λ_{ex} = 400nm, λ_{max} = 530nm) of the concentration dependent study of **L2** over the range (1×10^{-4}M to 1×10^{-6}M) recorded in H_2O. (**b**) Fluorescence emission spectra (λ_{ex} = 400nm, λ_{max} = 530nm) of **L2** over the concentration range (1×10^{-4}M to 1×10^{-6}M) recorded in CH_3CN. The sharp peak present in the lower concentration samples is a Raman scattering band from the solvent (Figure S23).*[S11]

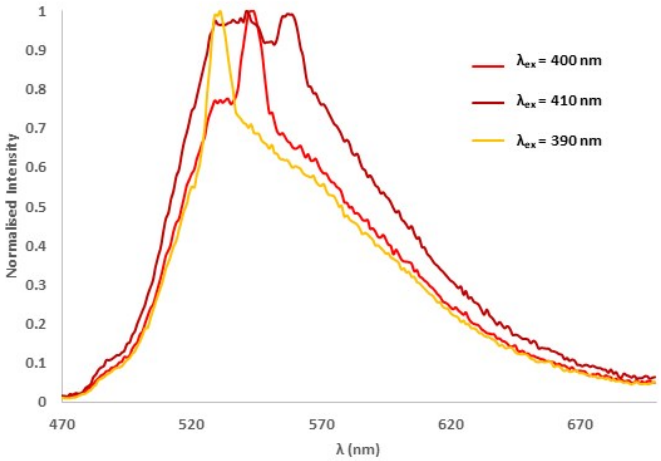

Fig. S23: (a) *Fluorescence emission spectra of **L2** (1×10^{-4}M) with λ_{ex} at 390 nm, 400nm and 410nm demonstrating dependence of the sharp feature in the emission spectra on the excitation wavelength, confirming that this is not a feature intrinsic to the emission spectrum of **L2**.*

pH titrations of L1

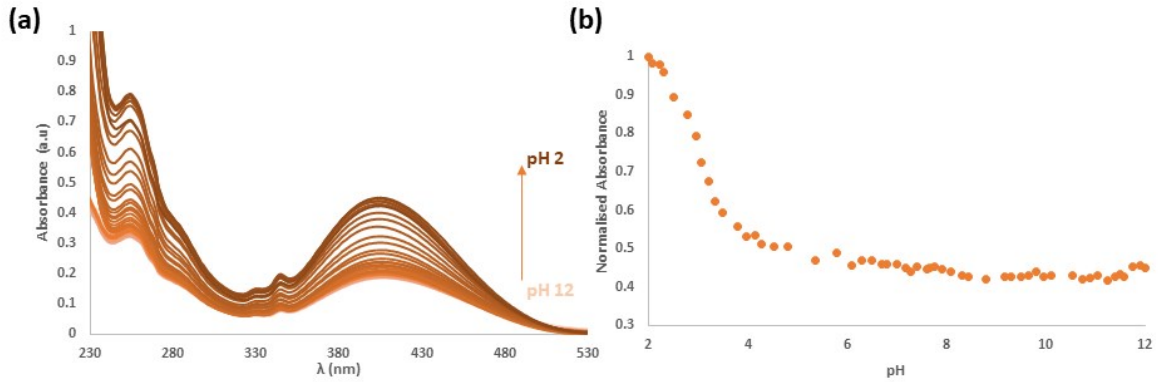

Fig S24: (a) *UV-Vis pH titration of **L1** of HCl$_{(aq)}$ at 0.1 pH unit intervals and initial NaOH $_{(aq)}$ base spike in 100 mM NaCl$_{(aq)}$ medium. (**b**) Normalised absorbance (λ_{max} = 400nm) of the titration.*

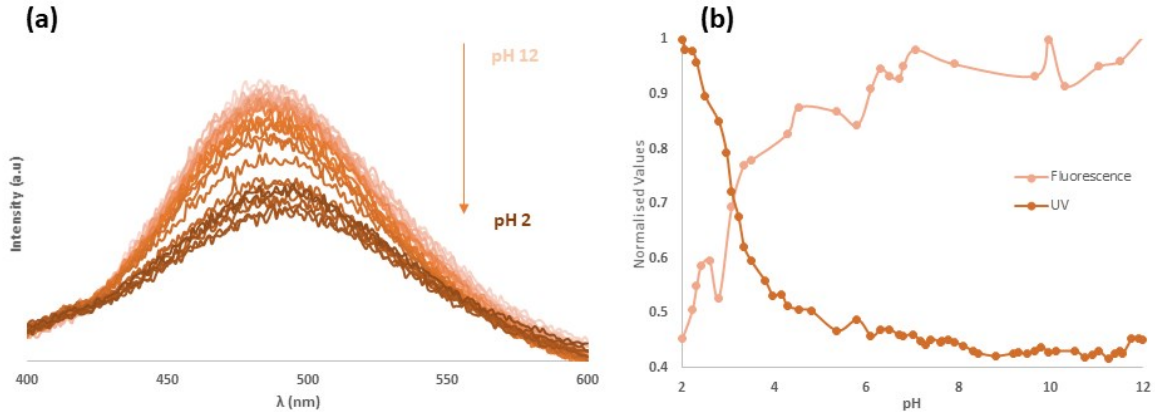

Fig. S25: *(**a**) Fluorescence pH titration of **L1** with additions of HCl$_{(aq)}$ at 0.1 pH unit intervals and an initial NaOH$_{(aq)}$ base spike in 100 mM NaCl$_{(aq)}$ medium. (**b**) Normalised absorbance (λ_{max} = 400nm) and fluorescence (λ_{ex} = 400nm, λ_{max} = 550nm) of the titration.*

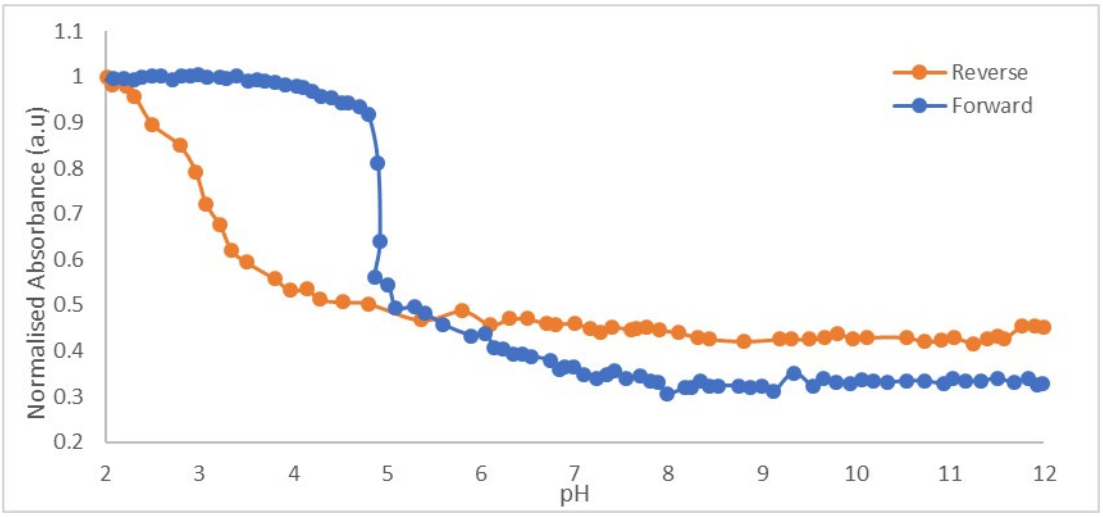

Fig S26: *Normalised absorbance (λ_{max} = 400nm) of the titration, illustrating the hysteresis effect in the system, with an initial $HCl_{(aq)}$ acid spike and additions of $NaOH_{(aq)}$ base spike from pH2 to pH12 (forward) and with an initial $NaOH_{(aq)}$ base spike and additions of $HCl_{(aq)}$ from pH12 to pH2 (reverse).*

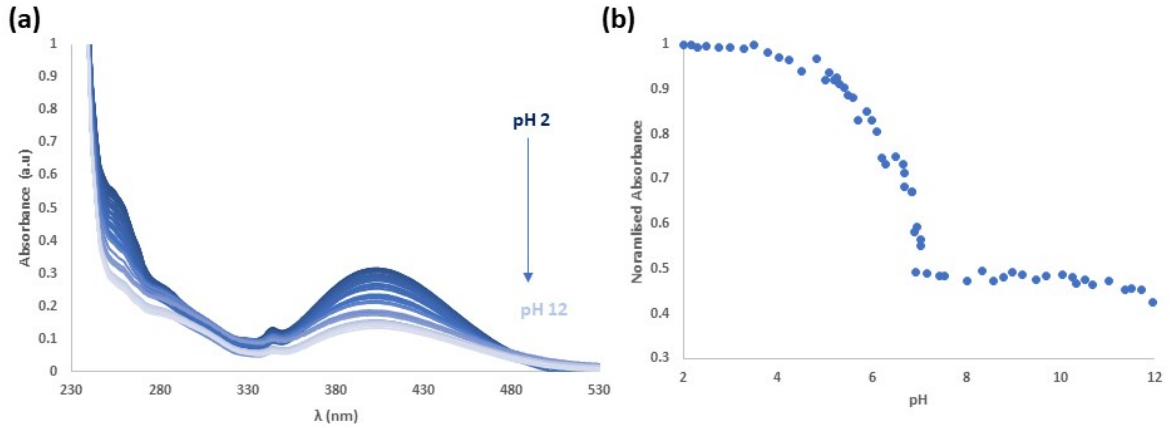

Fig S27: (a) *UV-Vis pH titration of **L1** with additions of $NaOH_{(aq)}$ at 0.1 pH unit intervals and initial $HNO_{3(aq)}$ acid spike in 100 mM $NaCl_{(aq)}$ medium. (**b**) Normalised absorbance (λ_{max} = 400nm) of the titration.*

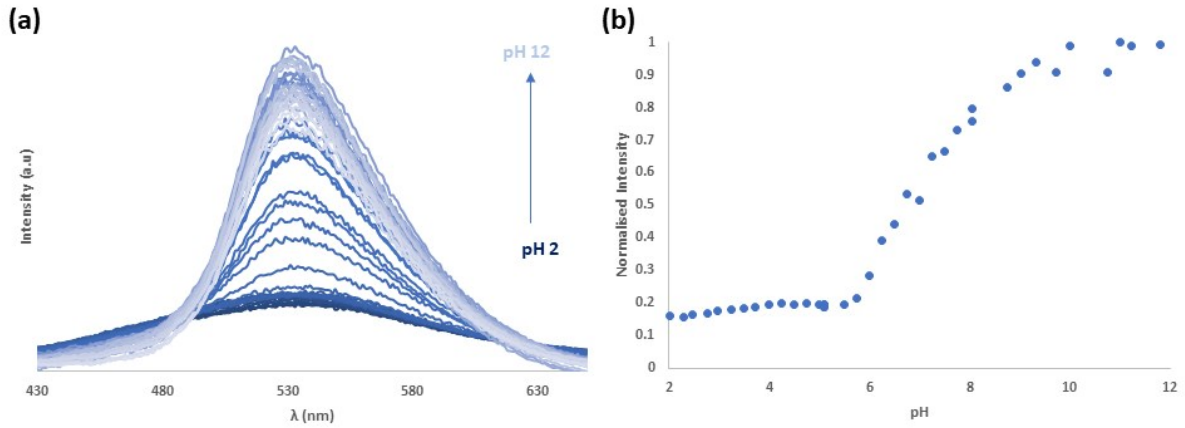

Fig. S28: ***(a)** Fluorescence pH titration of **L1** with additions of $NaOH_{(aq)}$ at 0.1 pH unit intervals and an initial $HNO_{3(aq)}$ acid spike in 100 mM $NaCl_{(aq)}$ medium. (**b**) Normalised fluorescence (λ_{ex} = 400nm, λ_{max} = 550nm) of the titration.*

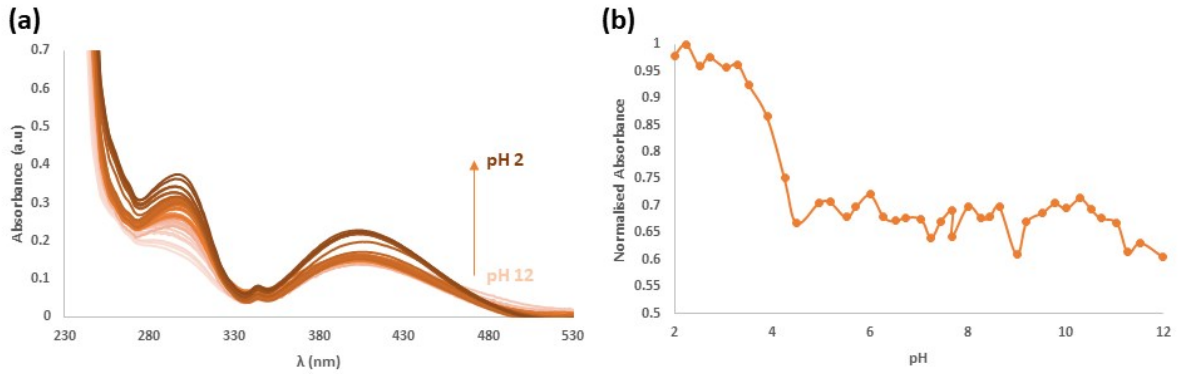

Fig. S29: *(**a**) UV-vis pH titration of **L1** with additions of $HNO_{3(aq)}$ at 0.1 pH unit intervals and an initial $NaOH_{(aq)}$ base spike in 100 mM $NaCl_{(aq)}$ medium. (**b**) Normalised absorbance (λ_{max} = 400nm) of the titration.*

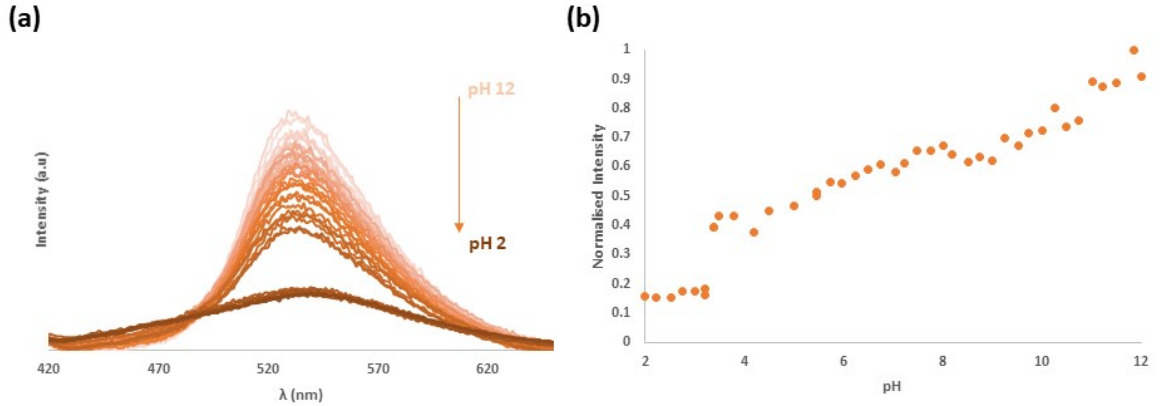

Fig. S30: (**a**) *Fluorescence pH titration of **L1** with additions of $HNO_{3(aq)}$ at 0.1 pH unit intervals and an initial $NaOH_{(aq)}$ base spike in 100 mM $NaCl_{(aq)}$ medium. (**b**) Normalised fluorescence (λ_{ex} = 400nm, λ_{max} = 550nm) of the titration.*

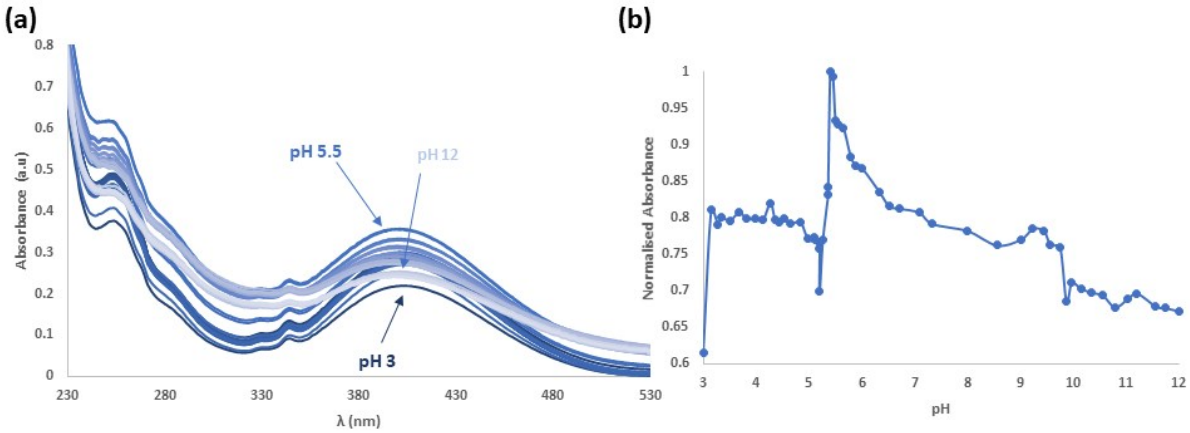

Fig S31: (**a**) *UV-Vis pH titration of **L1** with additions of $NaOH_{(aq)}$ at 0.1 pH unit intervals and initial $CH_3COOH_{(aq)}$ acid spike in 100 mM $NaCl_{(aq)}$ medium. (**b**) Normalised absorbance (λ_{max} = 400nm) of the titration.*

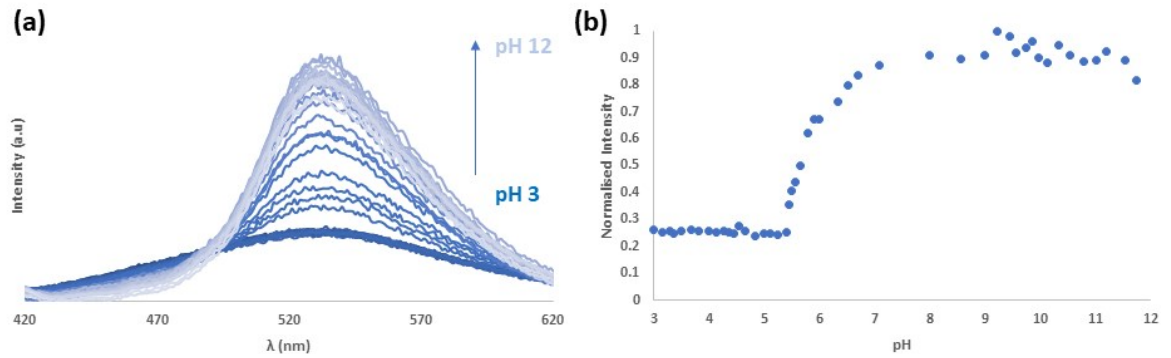

Fig. S32: *(**a**) Fluorescence pH titration of **L1** with additions of $NaOH_{(aq)}$ at 0.1 pH unit intervals and an initial $CH_3COOH_{(aq)}$ acid spike in 100 mM $NaCl_{(aq)}$ medium. (**b**) Normalised fluorescence (λ_{ex} = 400nm, λ_{max} = 550nm) of the titration.*

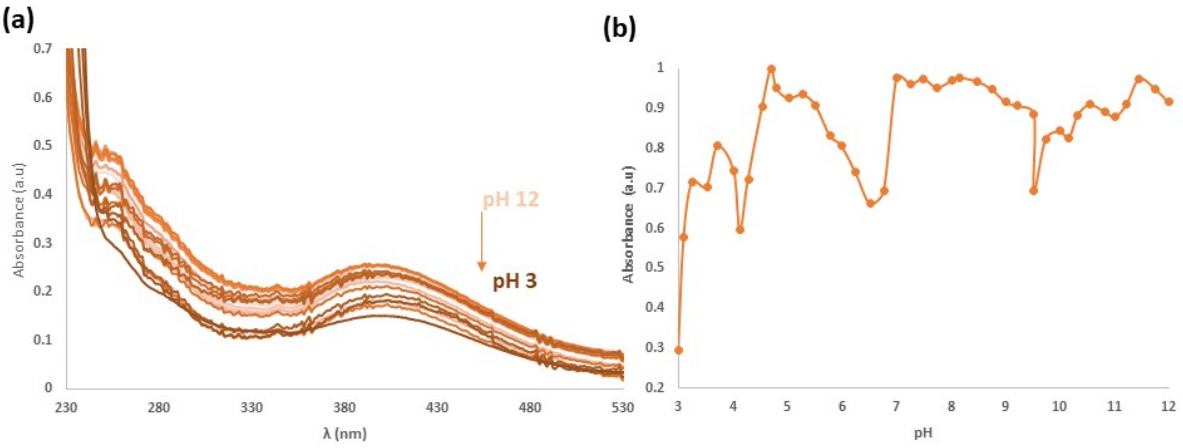

Fig. S33: *(**a**) UV-vis pH titration of **L1** with additions of $CH_3COOH_{(aq)}$ at 0.1 pH unit intervals and an initial $NaOH_{(aq)}$ base spike in 100 mM $NaCl_{(aq)}$ medium. (**b**) Normalised absorbance (λ_{max} = 400nm) of the titration.*

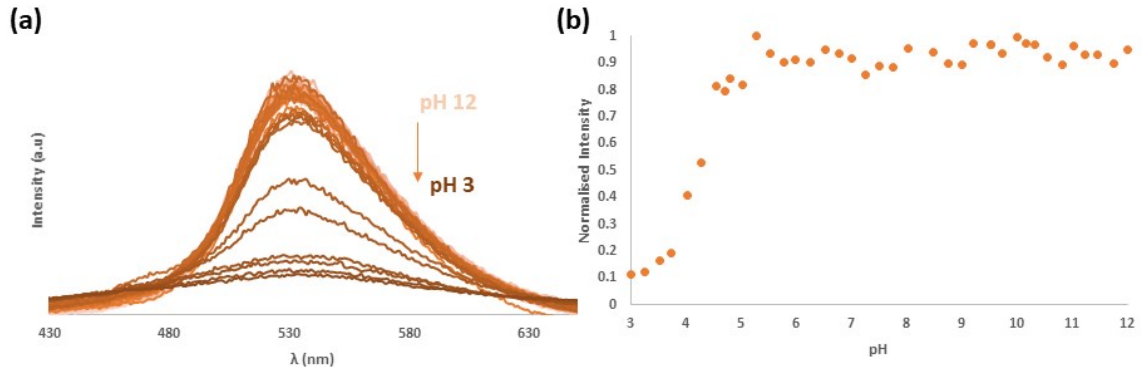

Fig. S34: (a) *Fluorescence pH titration of **L1** with additions of $CH_3COOH_{(aq)}$ at 0.1 pH unit intervals and an initial $NaOH_{(aq)}$ base spike in 100 mM $NaCl_{(aq)}$ medium. (**b**) Normalised fluorescence (λ_{ex} = 400nm, λ_{max} = 550nm) of the titration.*

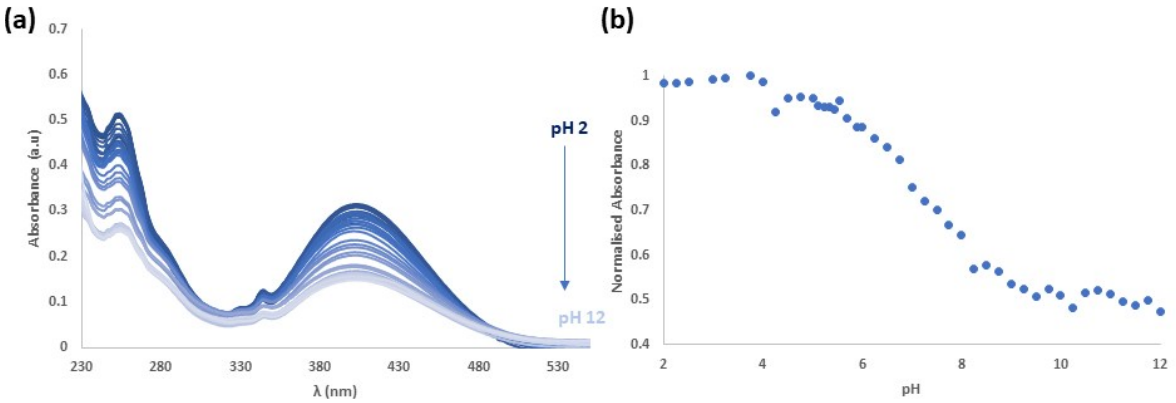

Fig. S35: *(**a**) UV-Vis pH titration of **L1** with additions of $NaOH_{(aq)}$ at 0.1 pH unit intervals and initial $HCl_{(aq)}$ acid spike in H_2O medium. (**b**) Normalised absorbance (λ_{max} = 400nm) of the titration.*

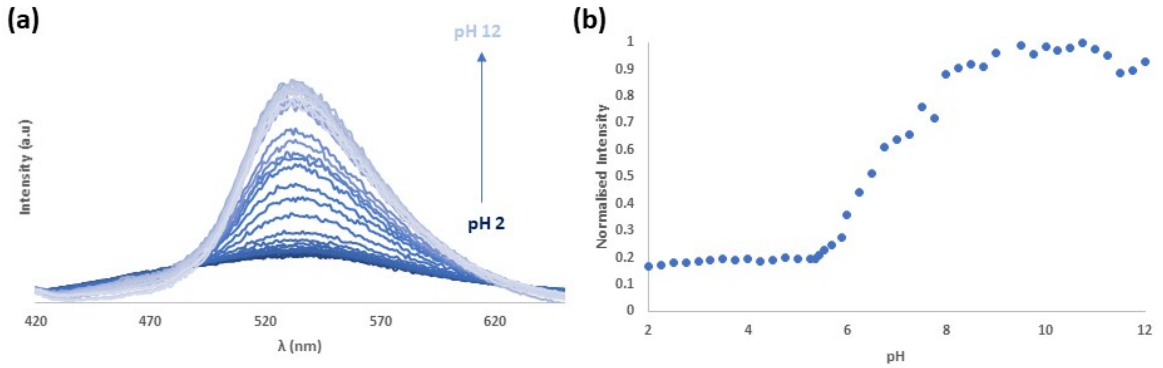

Fig. S36: *(**a**) Fluorescence pH titration of **L1** with additions of $NaOH_{(aq)}$ at 0.1 pH unit intervals and an initial $HCl_{(aq)}$ acid spike in H_2O medium. (**b**) Normalised fluorescence (λ_{ex} = 400nm, λ_{max} = 550nm) of the titration.*

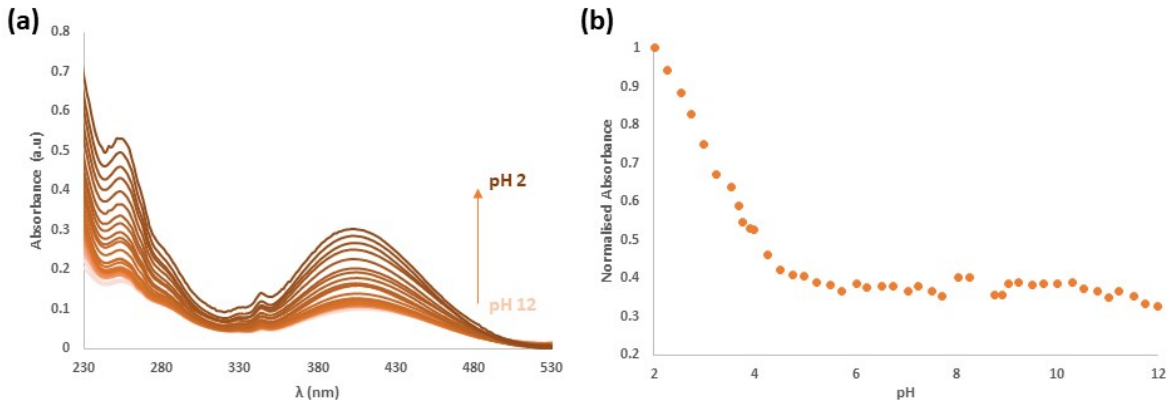

Fig. S37: *(**a**) UV-vis pH titration of **L1** with additions of $HCl_{(aq)}$ at 0.1 pH unit intervals and an initial $NaOH_{(aq)}$ base spike in H_2O medium. (**b**) Normalised absorbance (λ_{max} = 400nm) of the titration.*

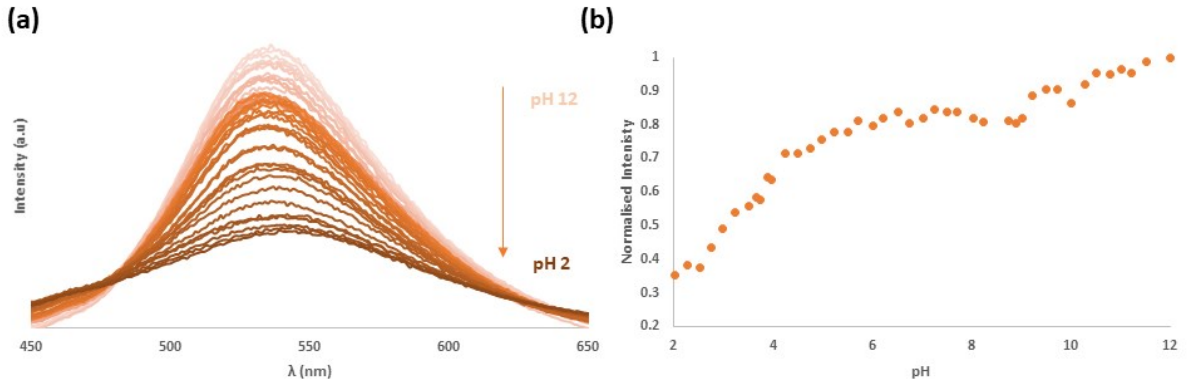

Fig. S38: (**a**) *Fluorescence pH titration of **L1** with additions of $HCl_{(aq)}$ at 0.1 pH unit intervals and an initial $NaOH_{(aq)}$ base spike in H_2O medium. (**b**) Normalised fluorescence (λ_{ex} = 400nm, λ_{max} = 550nm) of the titration.*

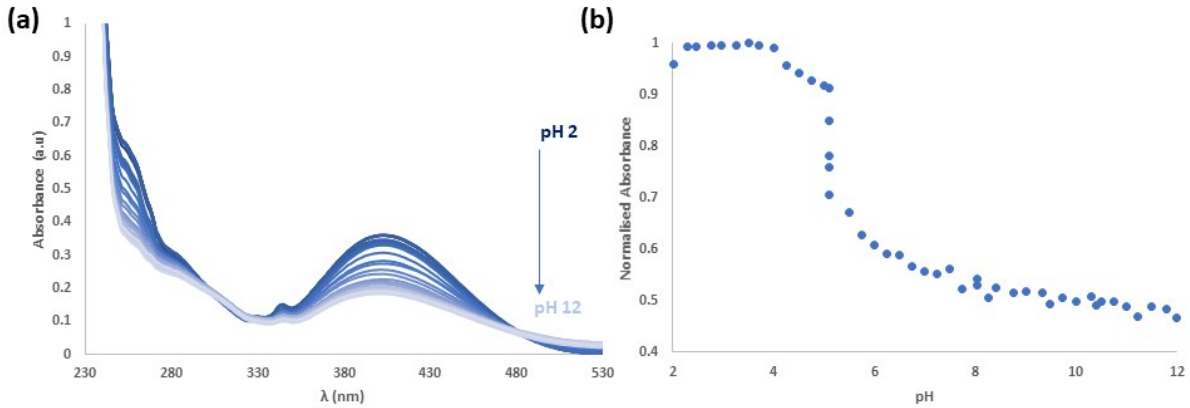

Fig. S39: *(**a**) UV-Vis pH titration of **L1** with additions of $NaOH_{(aq)}$ at 0.1 pH unit intervals and initial $HNO_{3\,(aq)}$ acid spike in H_2O medium. (**b**) Normalised absorbance (λ_{max} = 400nm) of the titration.*

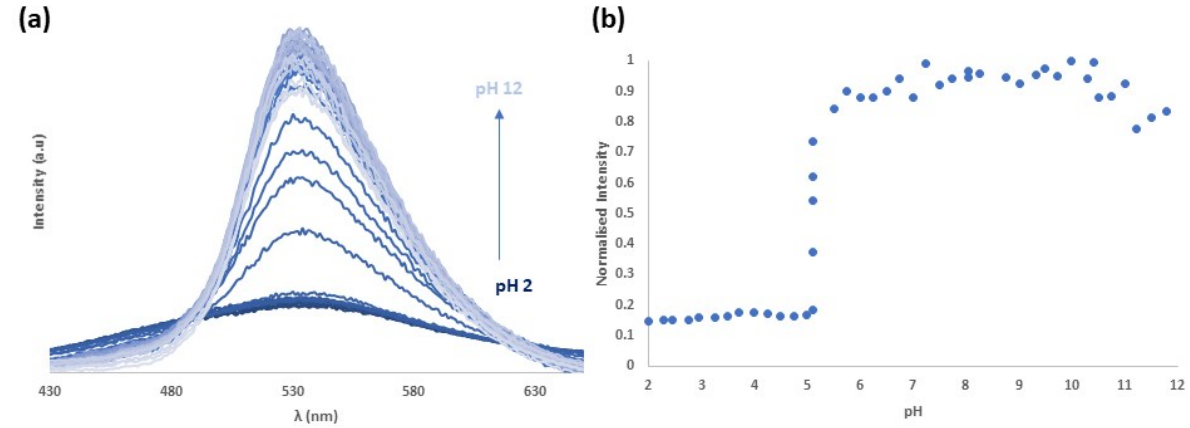

Fig. S40: *(**a**) Fluorescence pH titration of **L1** with additions of $NaOH_{(aq)}$ at 0.1 pH unit intervals and an initial $HNO_{3(aq)}$ acid spike in H_2O medium. (**b**) Normalised fluorescence (λ_{ex} = 400nm, λ_{max} = 550nm) of the titration.*

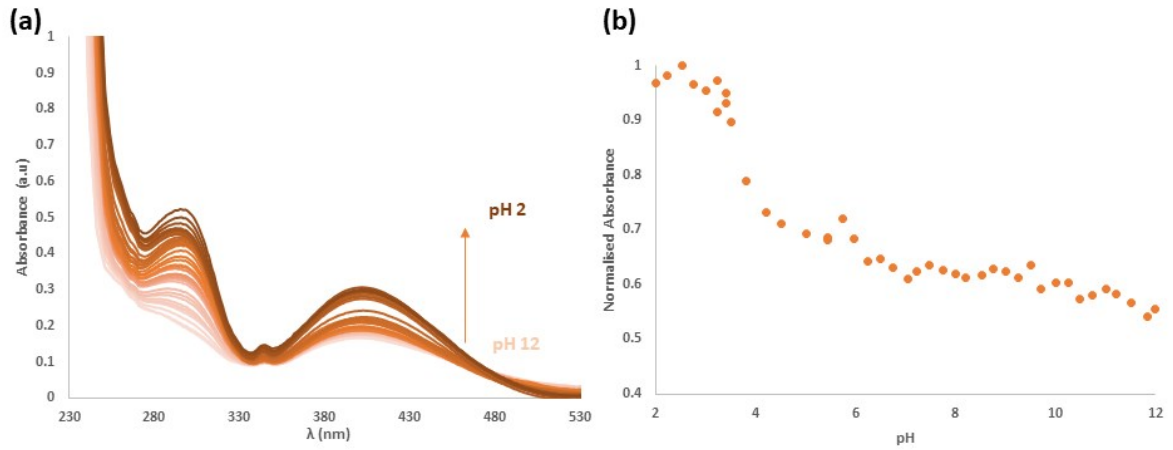

Fig. S41: *(**a**) UV-vis pH titration of **L1** with additions of $HNO_{3(aq)}$ at 0.1 pH unit intervals and an initial $NaOH_{(aq)}$ base spike in H_2O medium. (**b**) Normalised absorbance (λ_{max} = 400nm) of the titration.*

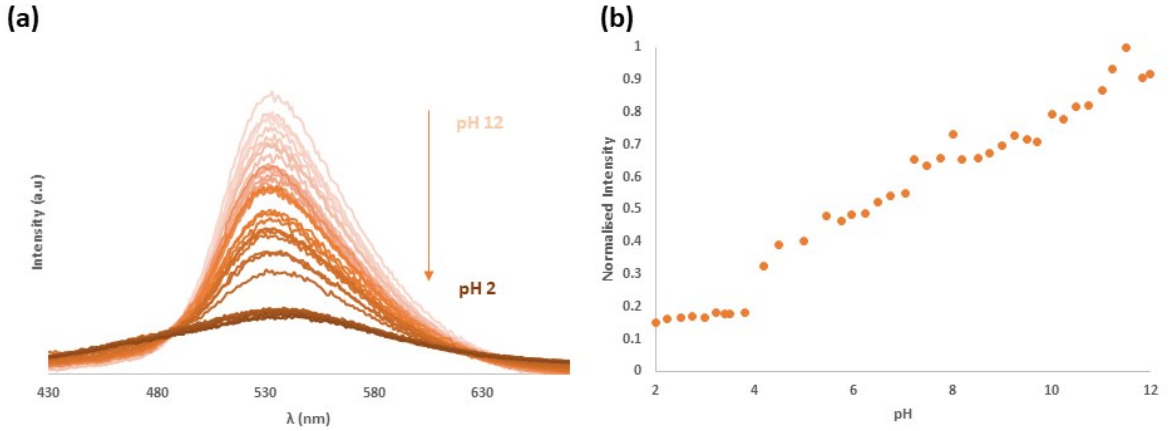

Fig. S42: (a) *Fluorescence pH titration of **L1** with additions of $HNO_{3(aq)}$ at 0.1 pH unit intervals and an initial $NaOH_{(aq)}$ base spike in H_2O medium. (**b**) Normalised fluorescence (λ_{ex} = 400nm, λ_{max} = 550nm) of the titration.*

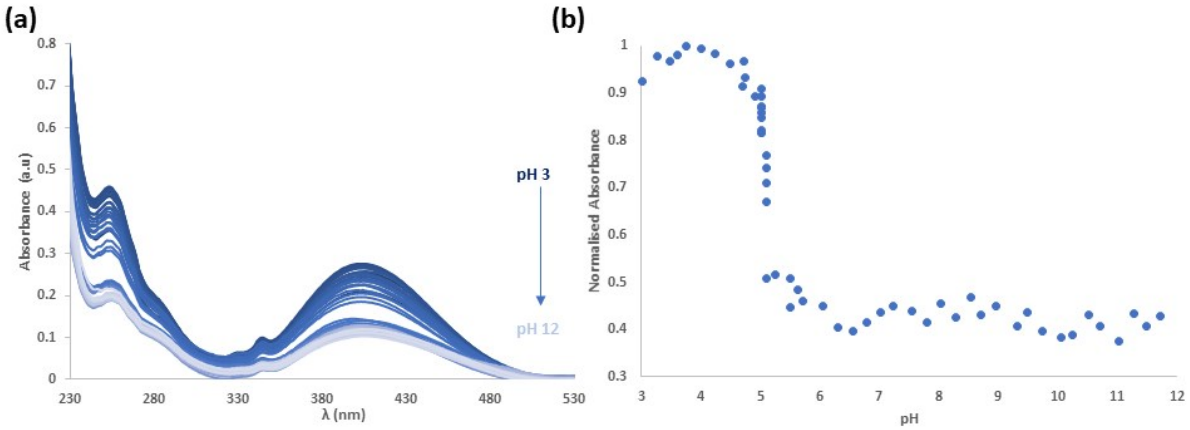

Fig. S43: (a) *UV-Vis pH titration of **L1** with additions of $NaOH_{(aq)}$ at 0.1 pH unit intervals and initial $CH_3COOH_{(aq)}$ acid spike in H_2O medium. (**b**) Normalised absorbance (λ_{max} = 400nm) of the titration.*

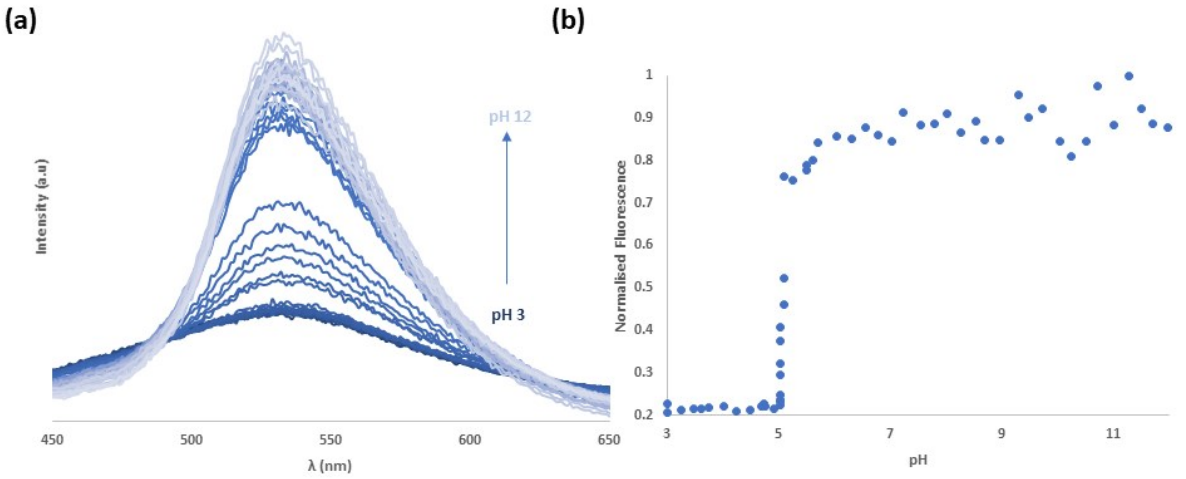

Fig. S44: *(**a**) Fluorescence pH titration of **L1** with additions of $NaOH_{(aq)}$ at 0.1 pH unit intervals and an initial $CH_3COOH_{(aq)}$ acid spike in H_2O medium. (**b**) Normalised fluorescence (λ_{ex} = 400nm, λ_{max} = 550nm) of the titration.*

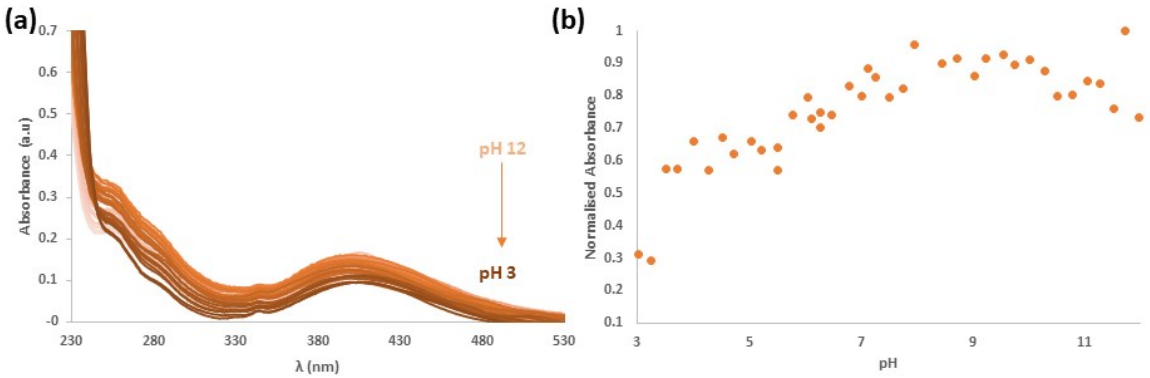

Fig. S45: *(**a**) UV-vis pH titration of **L1** with additions of $CH_3COOH_{(aq)}$ at 0.1 pH unit intervals and an initial $NaOH_{(aq)}$ base spike in H_2O medium. (**b**) Normalised absorbance (λ_{max} = 400nm) of the titration.*

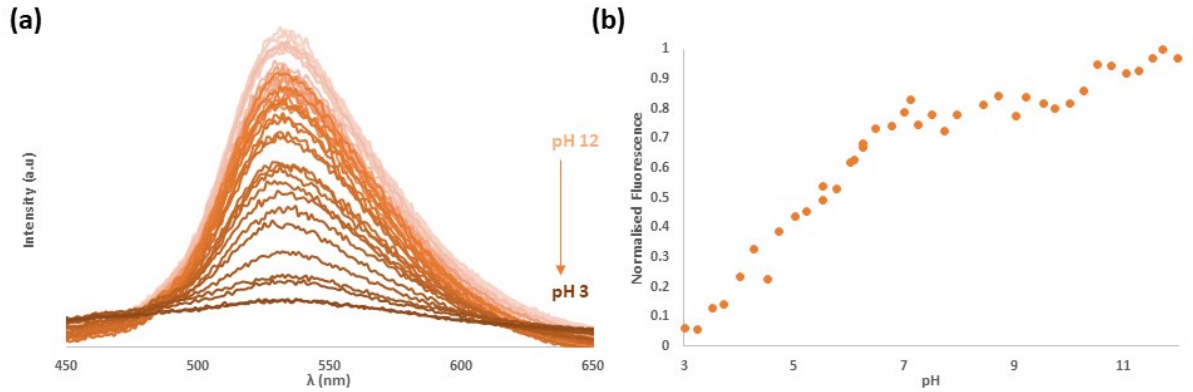

Fig. S46: (a) *Fluorescence pH titration of **L1** with additions of $CH_3COOH_{(aq)}$ at 0.1 pH unit intervals and an initial $NaOH_{(aq)}$ base spike in H_2O medium. (**b**) Normalised fluorescence (λ_{ex} = 400nm, λ_{max} = 550nm) of the titration.*

pH titrations of L2

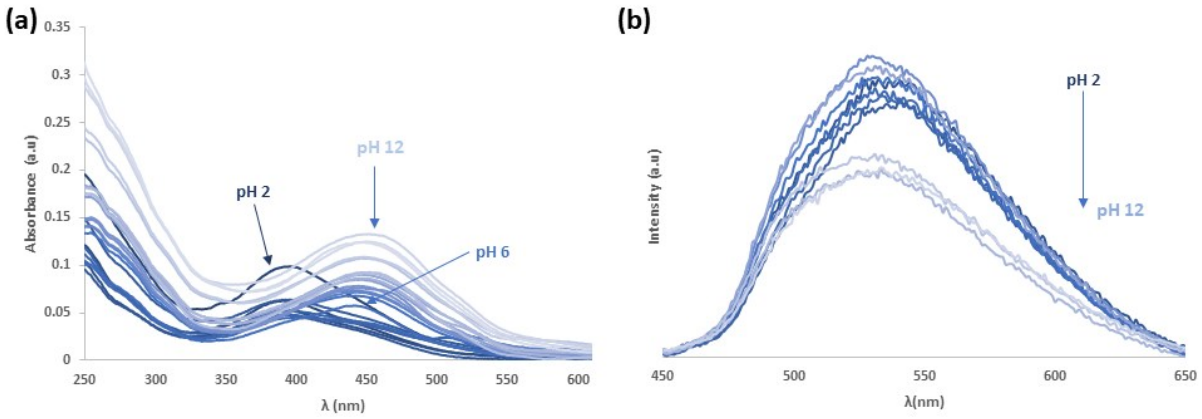

Fig. S47: *(**a**) UV-Vis pH titration of **L2** with additions of $NaOH_{(aq)}$ at 0.1 pH unit intervals and an initial $HCl_{(aq)}$ acid spike. (**b**) Fluorescence pH titration (λ_{ex} = 400nm) with additions of $NaOH_{(aq)}$ and an initial $HCl_{(aq)}$ acid spike in 100 mM $NaCl_{(aq)}$ medium.*

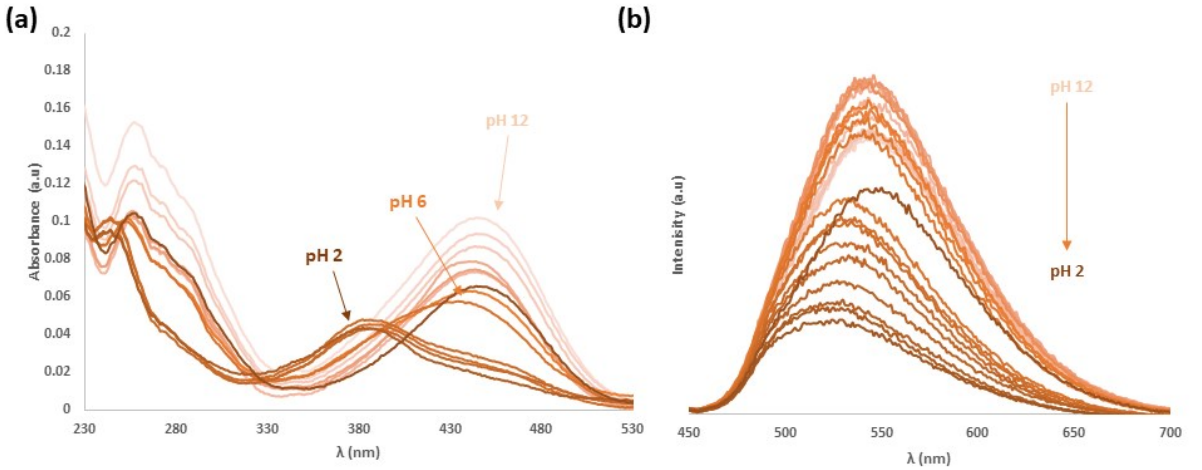

Fig. S48: (**a**) *UV-Vis pH titration of **L2** with additions of $HCl_{(aq)}$ at 0.1 pH unit intervals and initial $NaOH_{(aq)}$ base spike. (**b**) Fluorescence pH titration (λ_{ex} = 400nm) with additions of $HCl_{(aq)}$ and initial $NaOH_{(aq)}$ base spike in 100 mM $NaCl_{(aq)}$ medium.*

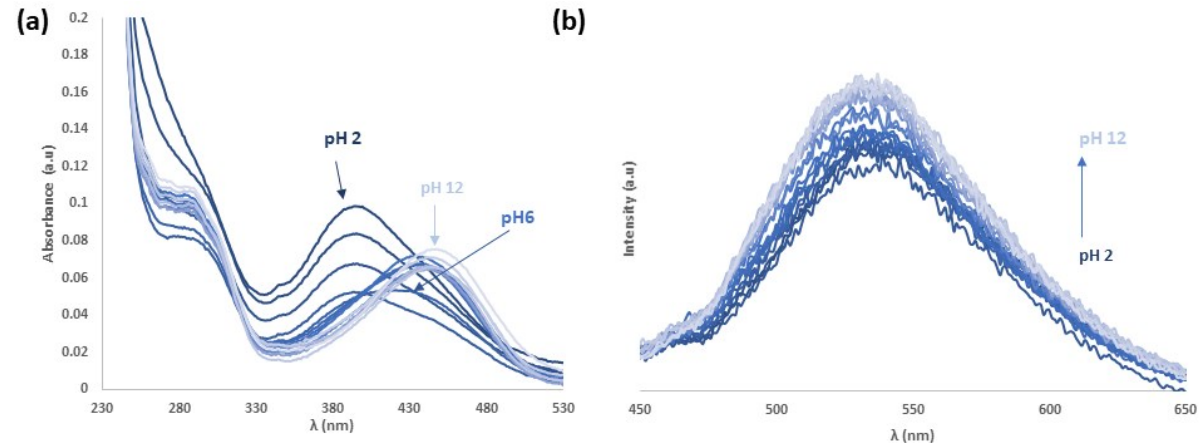

Fig. S49: (**a**) *UV-Vis pH titration of **L2** with additions of $NaOH_{(aq)}$ at 0.1 pH unit intervals and an initial $HNO_{3(aq)}$ acid spike. (**b**) Fluorescence pH titration (λ_{ex} = 400nm) with additions of $NaOH_{(aq)}$ and an initial $HNO_{3(aq)}$ acid spike in 100$mM_{(aq)}$ medium.*

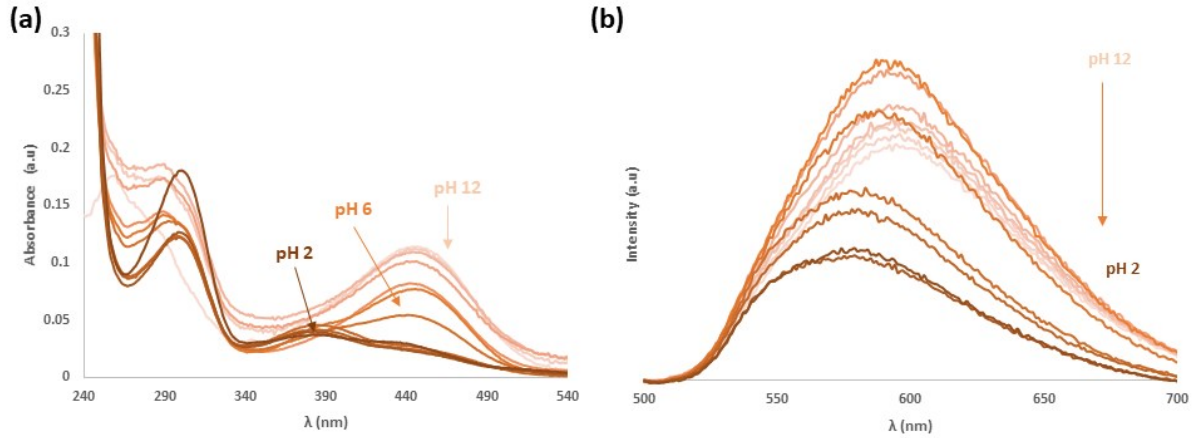

Fig. S50: *(a) UV-Vis pH titration of **L2** with additions of $HNO_{3\,(aq)}$ at 0.1 pH unit intervals and initial $NaOH_{(aq)}$ base spike. (**b**) Fluorescence pH titration (λ_{ex} = 450nm) with additions of $HNO_{3(aq)}$ and initial $NaOH_{(aq)}$ base spike in 100 mM $NaCl_{(aq)}$ medium.*

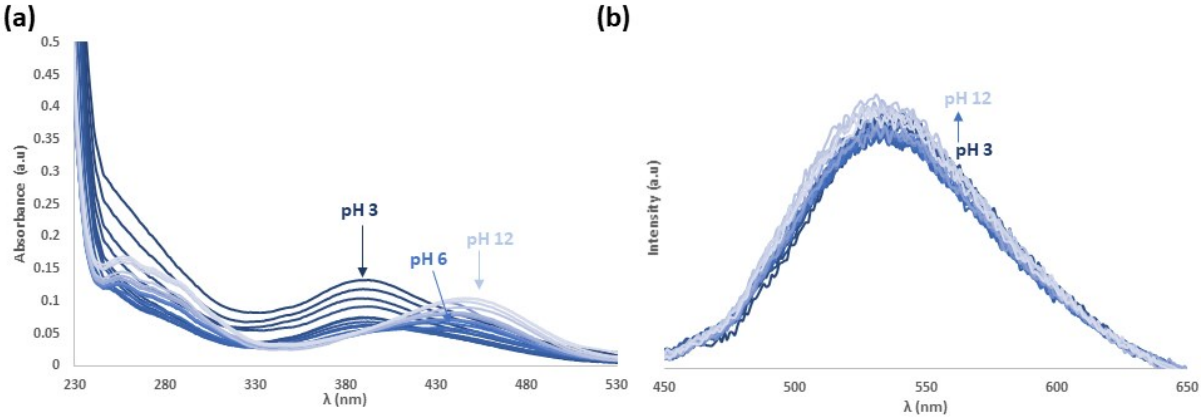

Fig. S51: *(**a**) UV-Vis pH titration of **L2** with additions of $NaOH_{(aq)}$ at 0.1 pH unit intervals and an initial $CH_3COOH_{(aq)}$ acid spike. (**b**) Fluorescence pH titration (λ_{ex} = 400nm) with additions of $NaOH_{(aq)}$ and an initial $CH_3COOH_{(aq)}$ acid spike in 100 mM medium.*

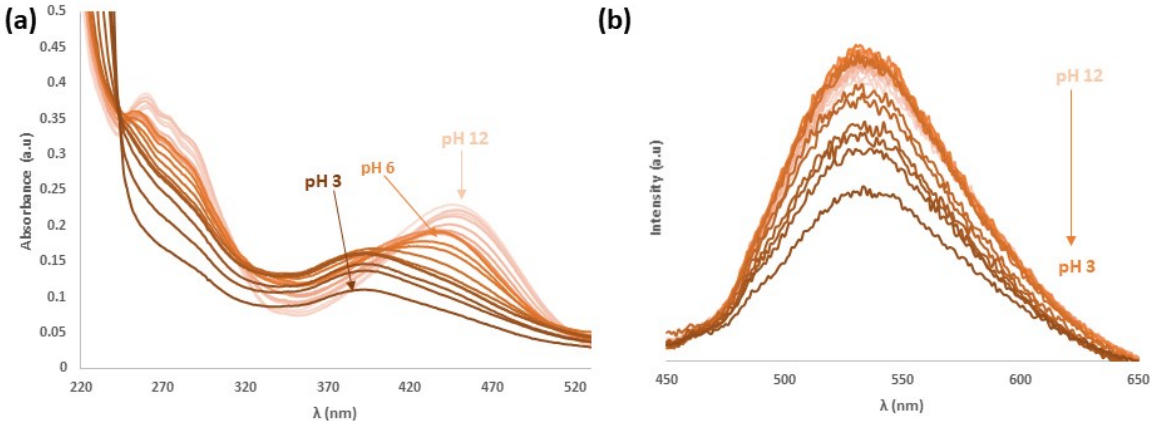

Fig. S52: *(**a**) UV-Vis pH titration of **L2** with additions of $CH_3COOH_{(aq)}$ at 0.1 pH unit intervals and initial $NaOH_{(aq)}$ base spike. (**b**) Fluorescence pH titration (λ_{ex} = 400nm) with additions of $CH_3COOH_{(aq)}$ and initial $NaOH_{(aq)}$ base spike in 100 mM $NaCl_{(aq)}$ medium.*

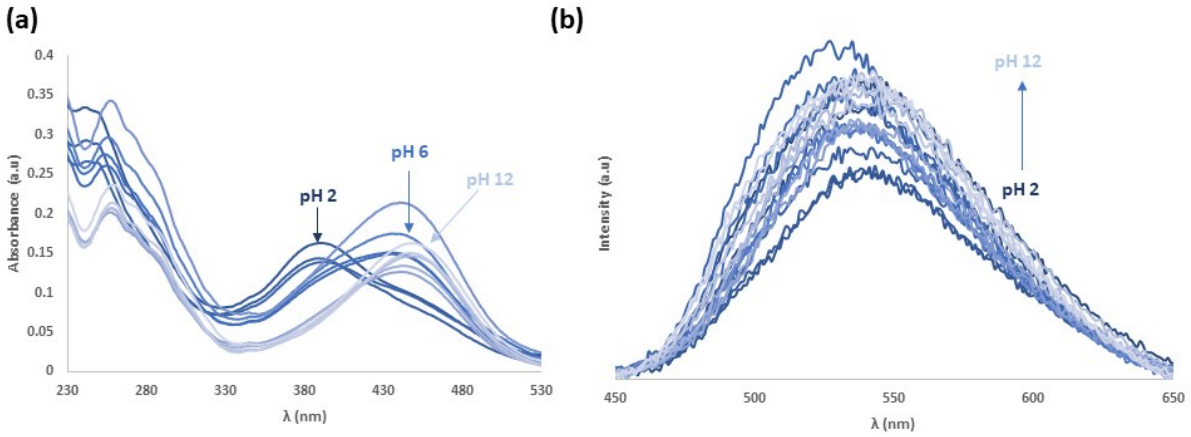

Fig. S53: *(**a**) UV-Vis pH titration of **L2** with additions of $NaOH_{(aq)}$ at 0.1 pH unit intervals and an initial $HCl_{(aq)}$ acid spike. (**b**) Fluorescence pH titration (λ_{ex} = 400nm) with additions of $NaOH_{(aq)}$ and an initial $HCl_{(aq)}$ acid spike in H_2O medium.*

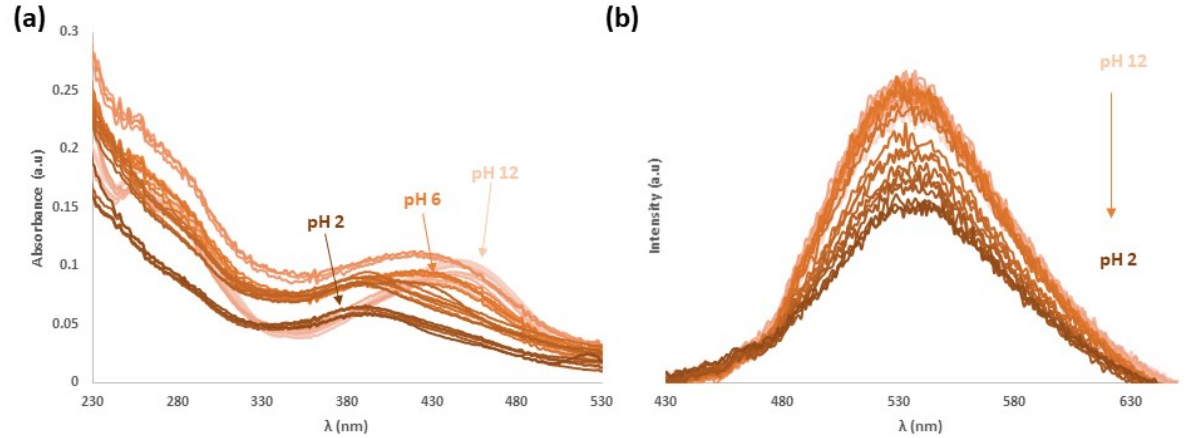

Fig.S54: *(**a**) UV-Vis pH titration of **L2** with additions of $CH_3COOH_{(aq)}$ at 0.1 pH unit intervals and initial $NaOH_{(aq)}$ base spike. (**b**) Fluorescence pH titration (λ_{ex} = 400nm) with additions of $CH_3COOH_{(aq)}$ and initial $NaOH_{(aq)}$ base spike in H_2O medium.*

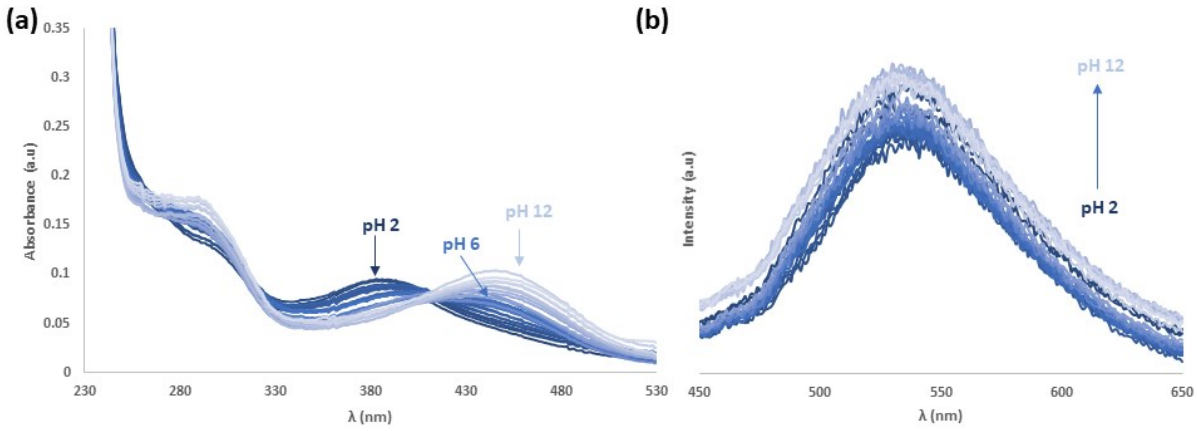

Fig. S55: *(**a**) UV-Vis pH titration of **L2** with additions of $NaOH_{(aq)}$ at 0.1 pH unit intervals and an initial $HNO_{3(aq)}$ acid spike. (**b**) Fluorescence pH titration (λ_{ex} = 400nm) with additions of $NaOH_{(aq)}$ and an initial $HNO_{3(aq)}$ acid spike in H_2O medium.*

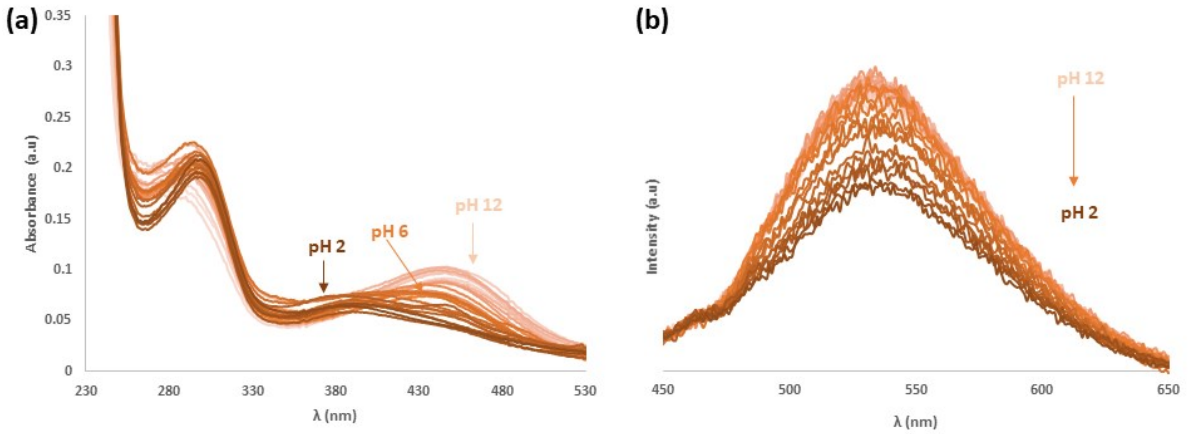

Fig. S56: *(**a**) UV-Vis pH titration of **L2** with additions of $HNO_{3\,(aq)}$ at 0.1 pH unit intervals and initial $NaOH_{(aq)}$ base spike. (**b**) Fluorescence pH titration (λ_{ex} = 400nm) with additions of $HNO_{3(aq)}$ and initial $NaOH_{(aq)}$ base spike in H_2O medium.*

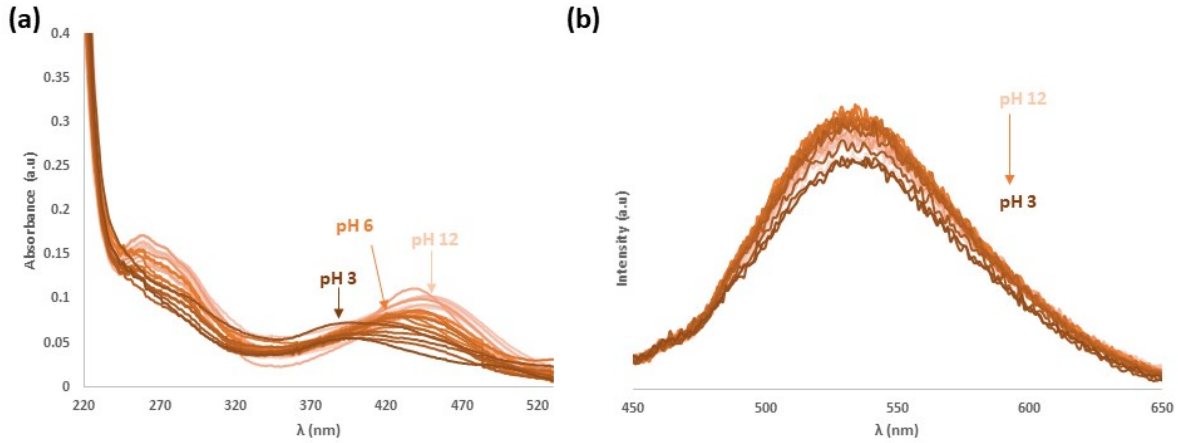

Fig. S57: *(a) UV-Vis pH titration of **L2** with additions of $CH_3COOH_{\,(aq)}$ at 0.1 pH unit intervals and initial $NaOH_{(aq)}$ base spike. (**b**) Fluorescence pH titration (λ_{ex} = 400nm) with additions of $CH_3COOH_{(aq)}$ and initial $NaOH_{(aq)}$ base spike in H_2O medium.*

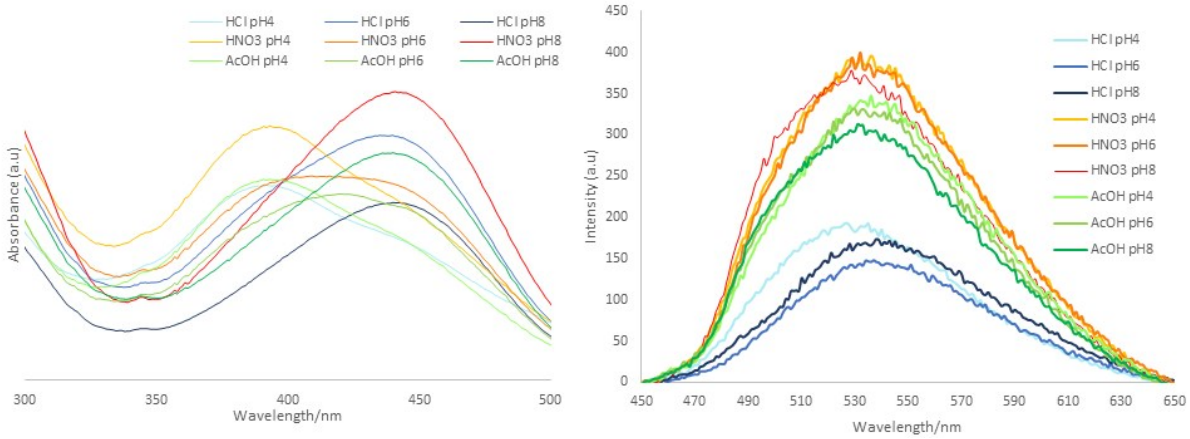

Fig. S58: *Effect of counterion at pH4, 6 and 8 for **L2**.*

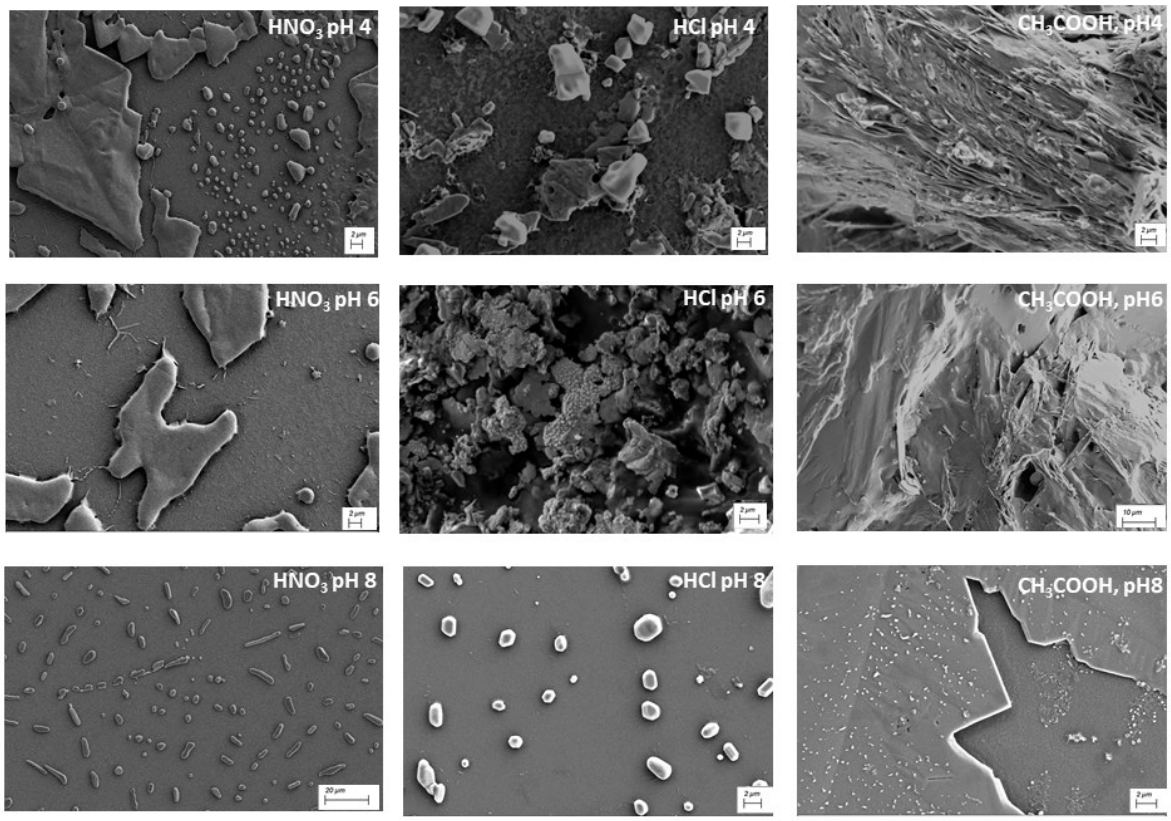

Fig. S59*: SEM images of* ***L1*** *aggregates.*

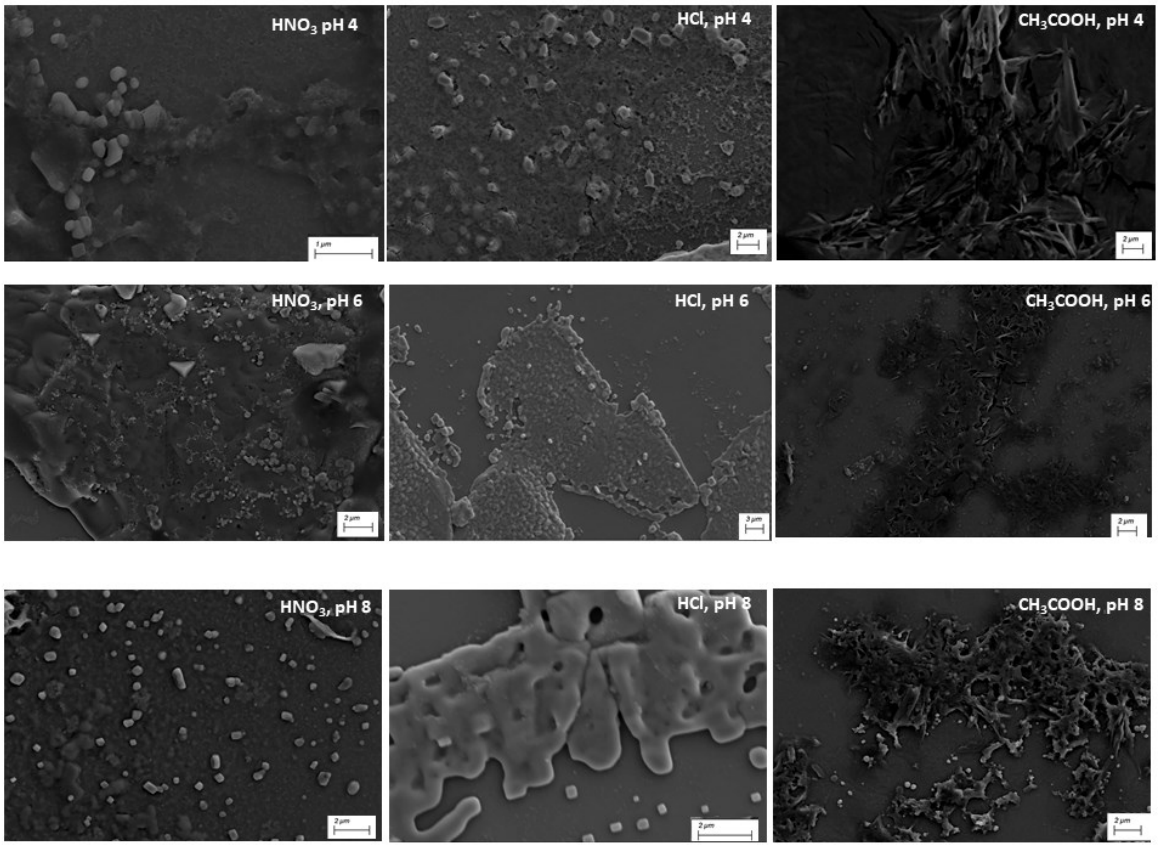

Fig. S60*: SEM images of* ***L2*** *aggregates.*

Table S4: *Wt% and Decomposition Temperature of Gel **1** (Mn-L1) and gel **2** (Co-L1).*

Gel	Wt%	Decomposition temperature/°C
1	1.0	52 - 54
2	0.9	74 - 76

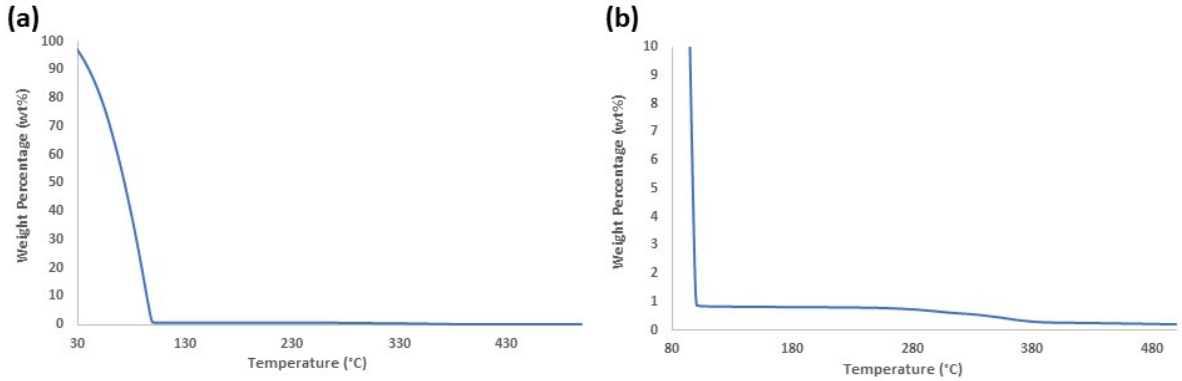

Fig.S61: (**a**) *Thermogravimetric analysis of gel **1** (Mn-**L1**) with inset (b).*

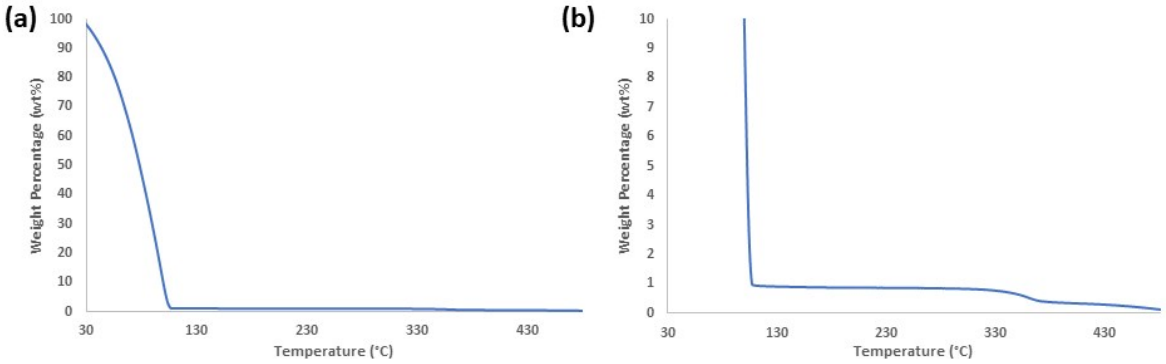

Fig. S62: (**a**) *Thermogravimetric analysis of gel **2**(Co-**L1**) with inset (b).*

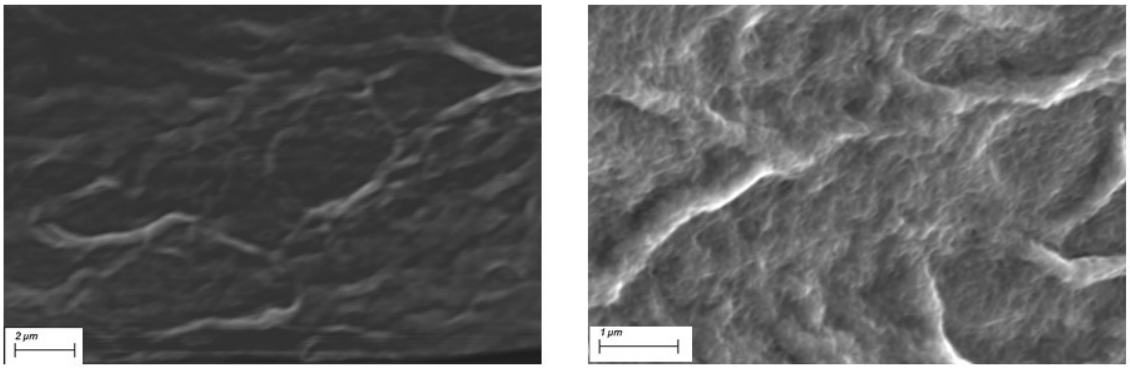

Fig. S63: *SEM images of gel **1** illustrating the fibrous morphology.*

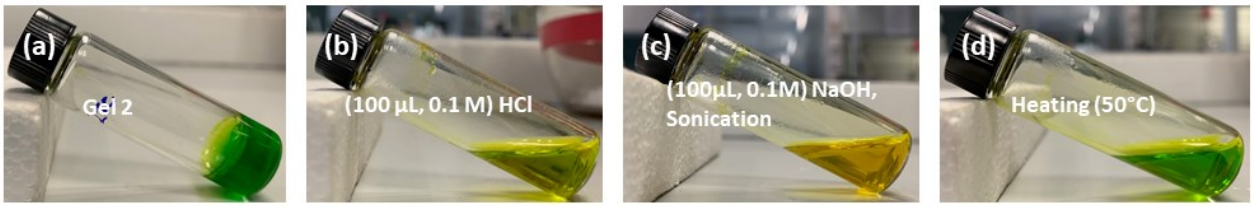

Fig. S64: *pH responsiveness of gel **2**: (**a**) gel **2** (**L1**-Co), (**b**) decomposition of gel after addition of $HCl_{(aq)}$, (**c**) addition of $NaOH_{(aq)}$, (**d**) heating of sample elucidating a thermochromic response.*

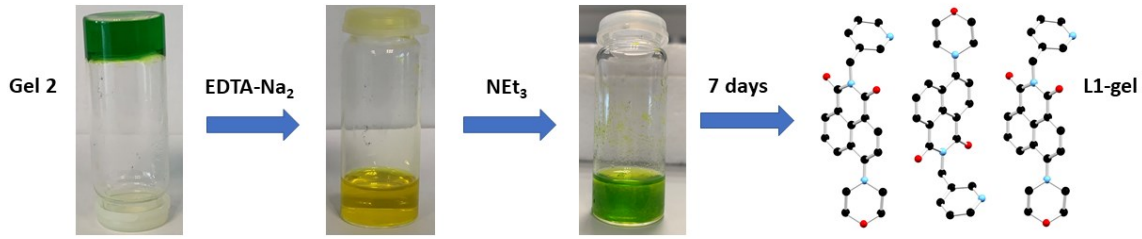

Fig. S65: *Metal sequestration experiment of gel **2**.*

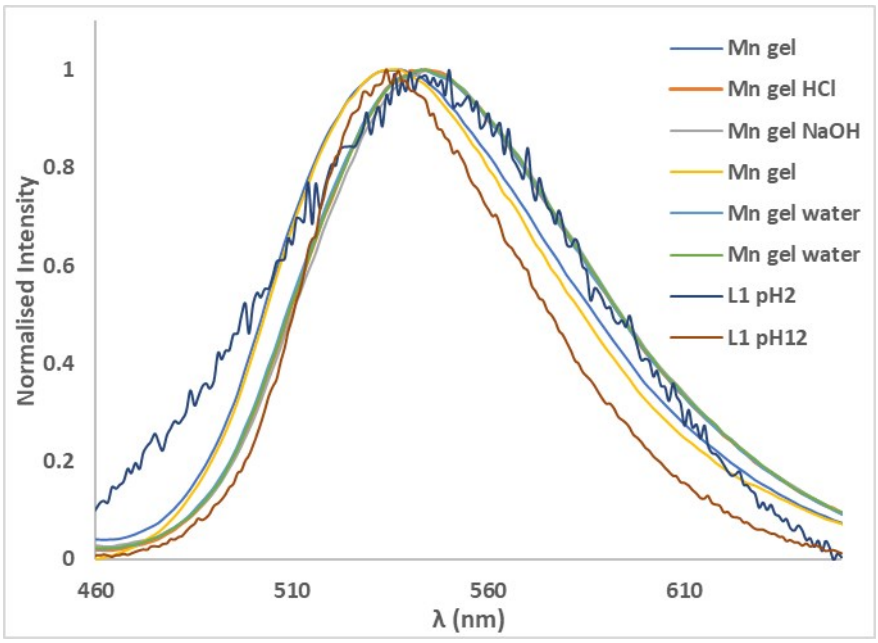

Fig. S66: *Normalised solid-state fluorescence (λ_{ex} = 400nm) of gel **1**.*

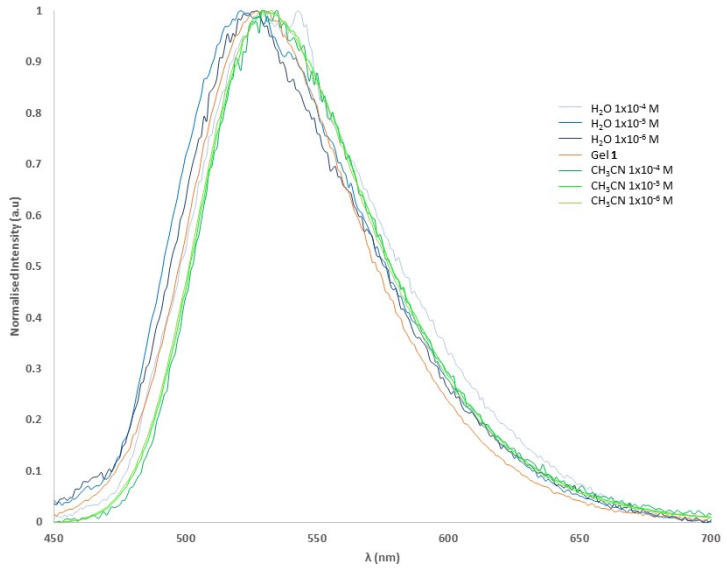

Fig. S67: *Normalised fluorescence emission spectra (λ_{ex} = 400nm) of gel **1** and **L1** over the concentration range of 1×10^{-4}M to 1×10^{-6}M recorded in CH_3CN and H_2O.*

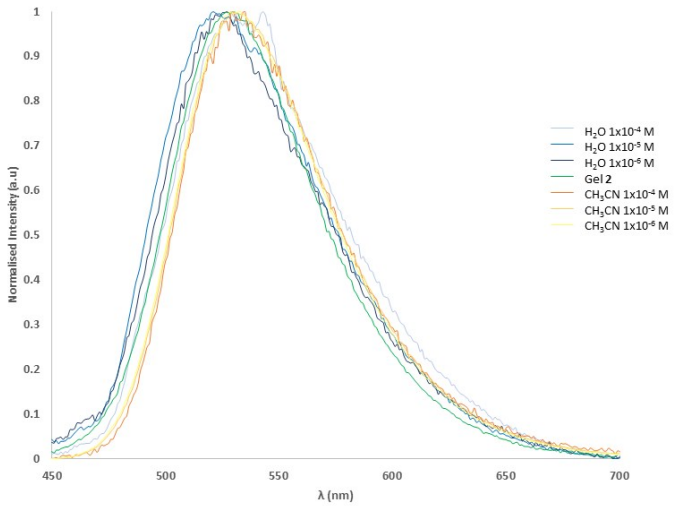

Fig S68: *Normalised fluorescence emission spectra (λ_{ex} = 400nm) of gel **2** and **L1** over the concentration range of 1×10^{-4}M to 1×10^{-6}M recorded in CH_3CN and H_2O.*

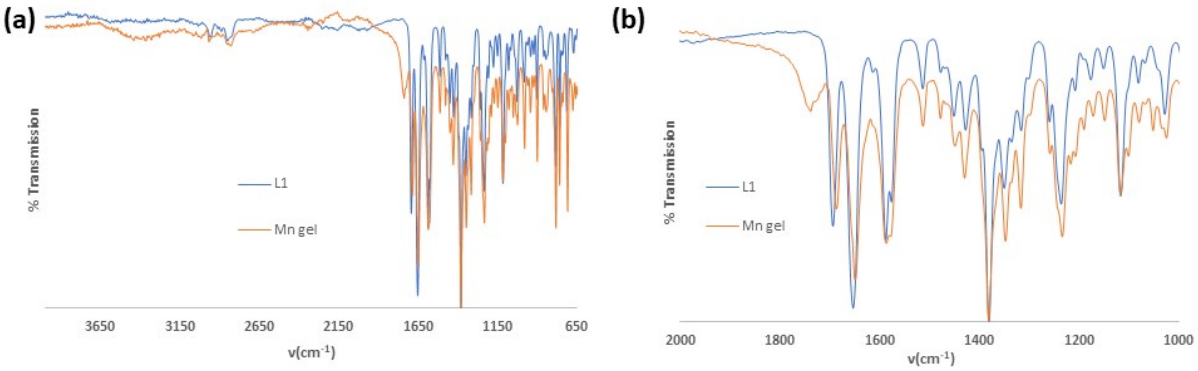

Fig S69: (a) *FTIR spectra of gel **1** overlaid with the free ligand spectra of **L1**, (**b**) Expanded FTIR spectra of gel **1** overlaid with the free ligand spectra of **L1**.*

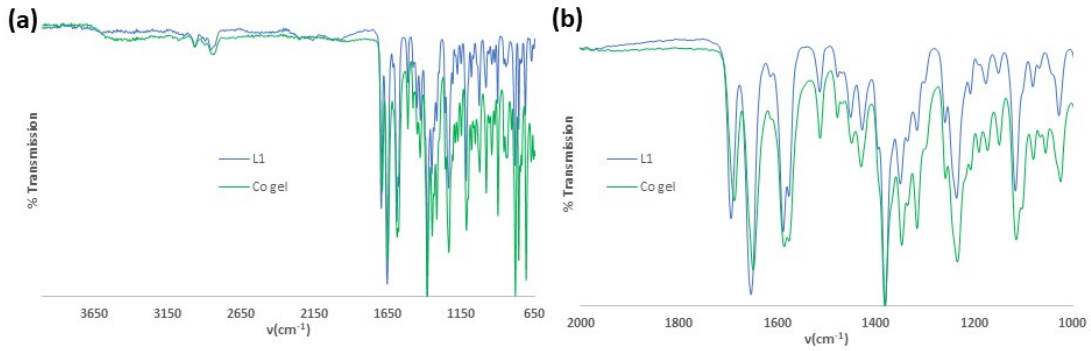

Fig S70: *FTIR spectra of gel **2** overlaid with the free ligand spectra of **L1**, (**b**) Expanded FTIR spectra of gel **2** overlaid with the free ligand spectra of **L1**.*

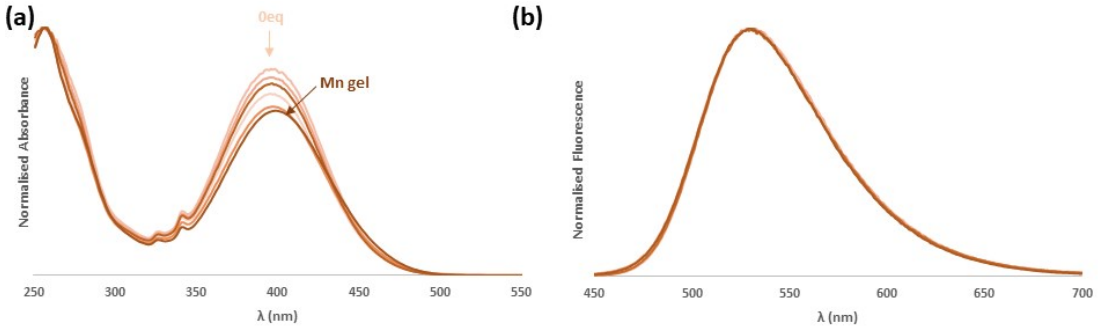

Fig S71: (a) *Normalised UV-vis absorption spectra of **L1** overlaid with spectra of 0.2eq aliquot additions of Mn(II) and gel **1** spectra. (**b**) Normalised Fluorescence spectra (λ_{ex} = 400nm) spectra of **L1** overlaid with spectra of 0.2eq aliquot additions of Mn(II) and gel **1** spectra.*

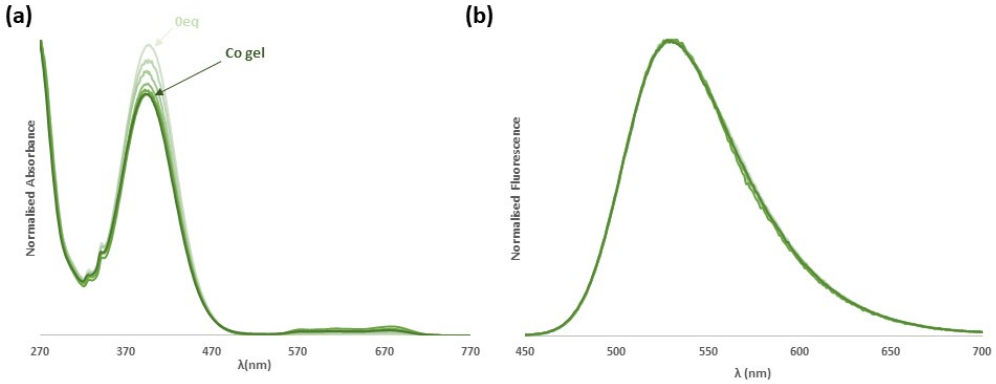

Fig S72: (a) *Normalised UV-vis absorption spectra of **L1** overlaid with spectra of 0.2eq aliquot additions of Co(II) and gel **2** spectra. (**b**) Normalised Fluorescence spectra (λ_{ex} = 400nm) spectra of **L1** overlaid with spectra of 0.2eq aliquot additions of Co(II) and gel **2** spectra.*

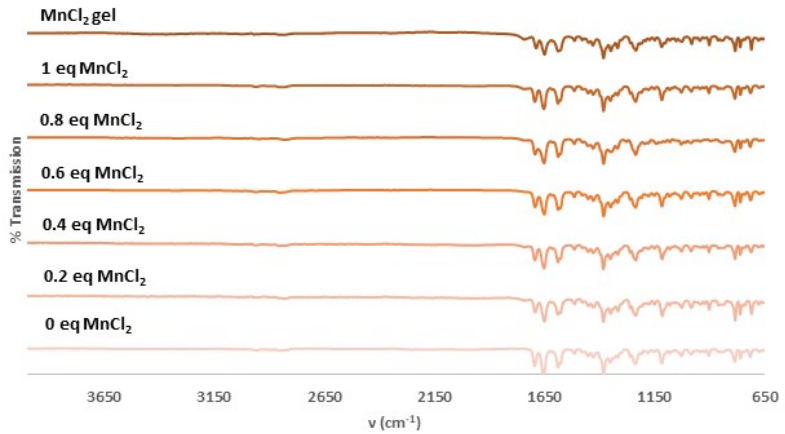

Fig S73: *FTIR spectra of **L1**, overlaid with spectra of various M:L mixtures and gel **1**.*

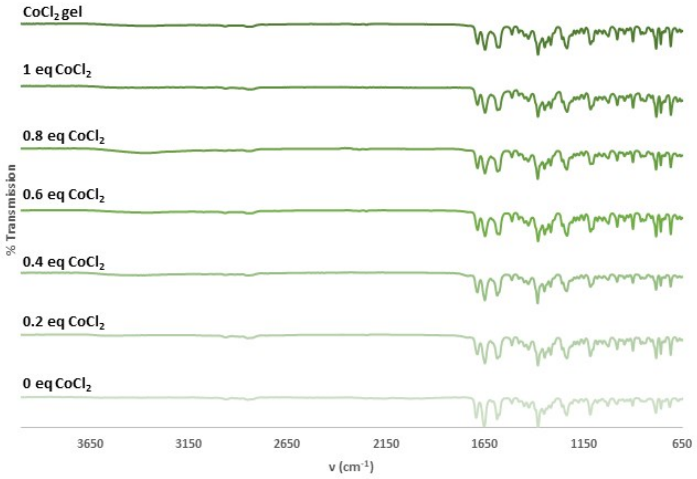

Fig S74: *FTIR spectra of **L1**, overlaid with spectra of various M:L mixtures and gel **2**.*

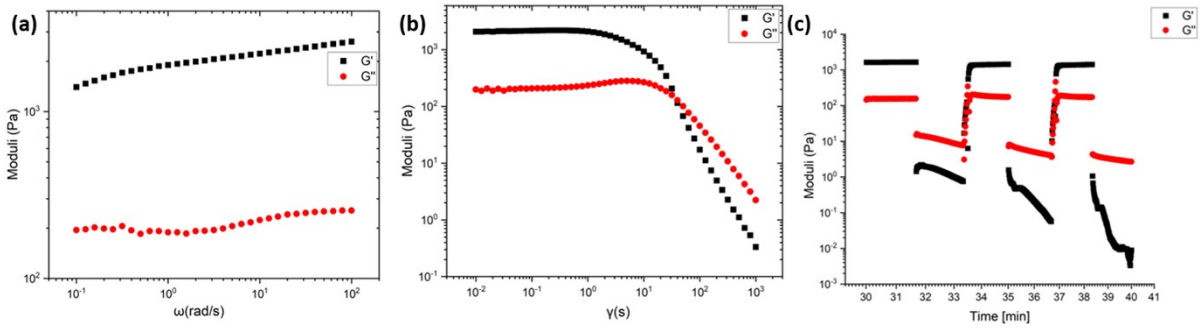

Fig. S75: *Rheological studies for gel **1** prepared at 1.7 wt% in acetonitrile, showing **(a)** frequency sweep over consecutive cycles (γ = 0.1%) **(b)** amplitude sweep (ω = 1 rad s^{-1}) and **(c)** recovery test at alternating 0.1% and 500% strain amplitudes.*

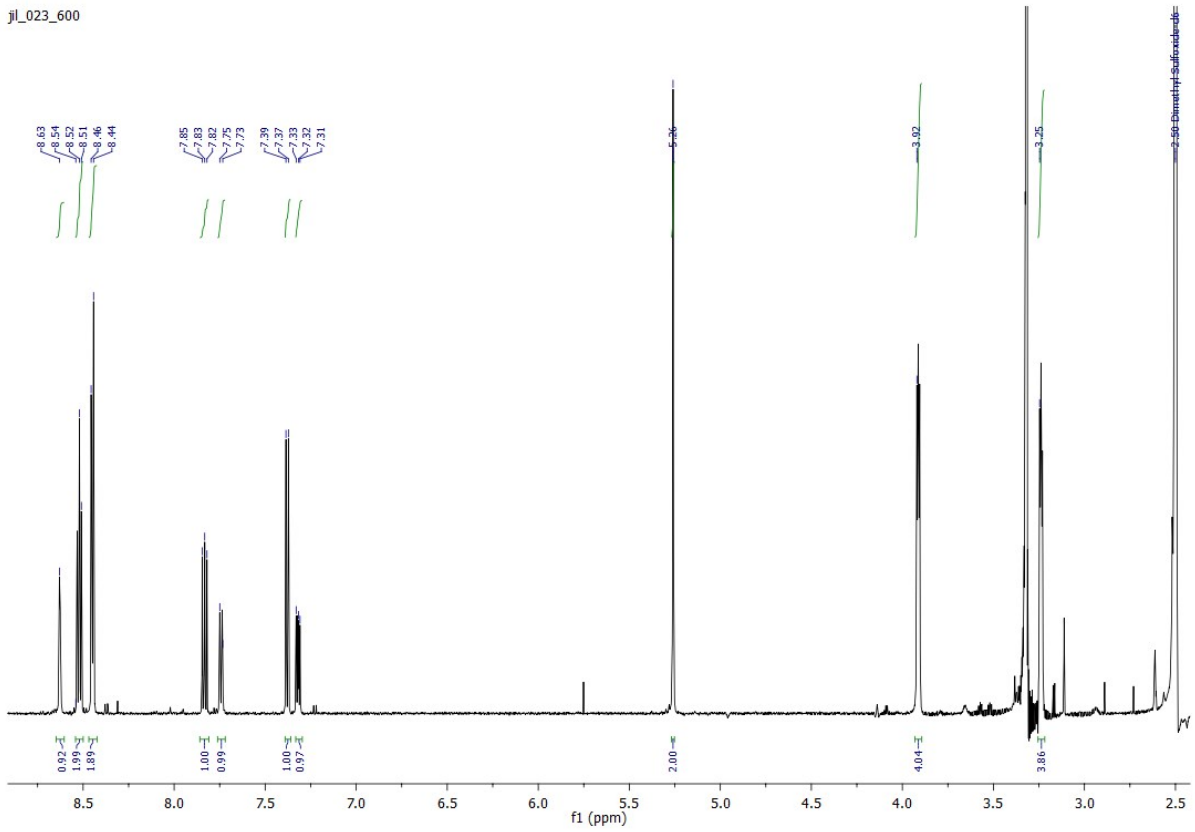

Fig. S76: *[1]H NMR spectrum for **L1.***

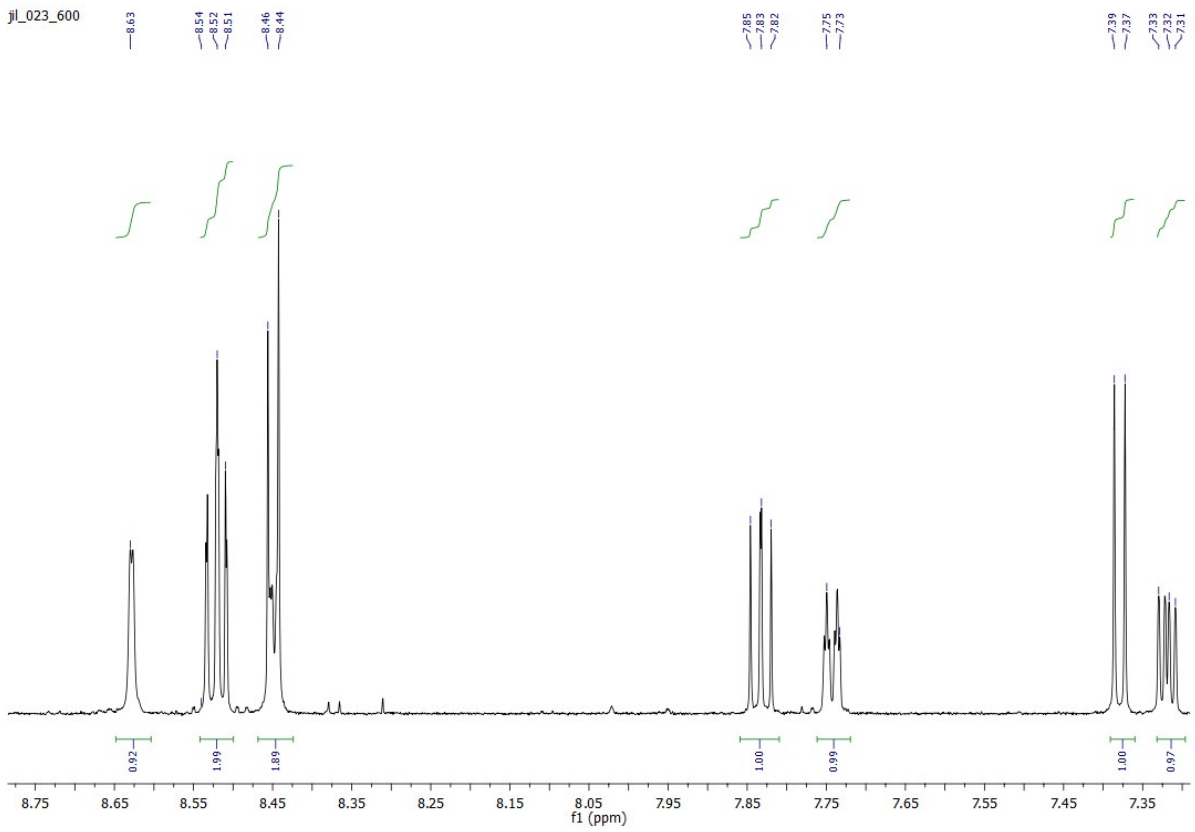

Fig. S77: *[1]H NMR spectrum with expanded aromatic region for **L1.***

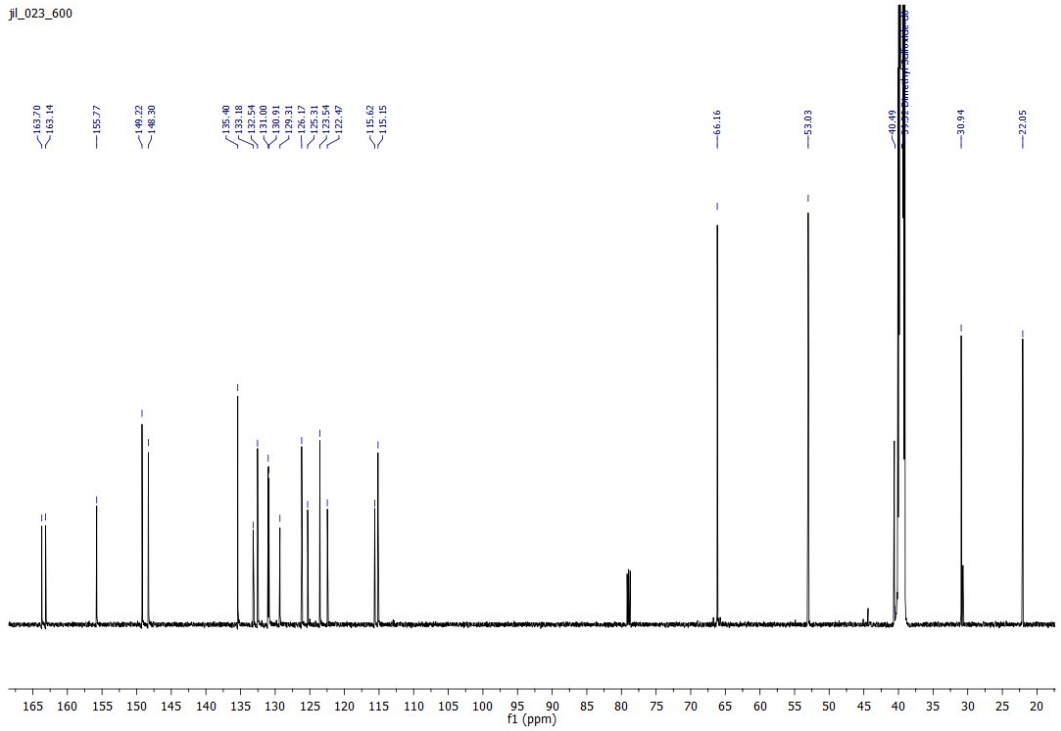

Fig. S78: *[13]C NMR spectrum for **L1***

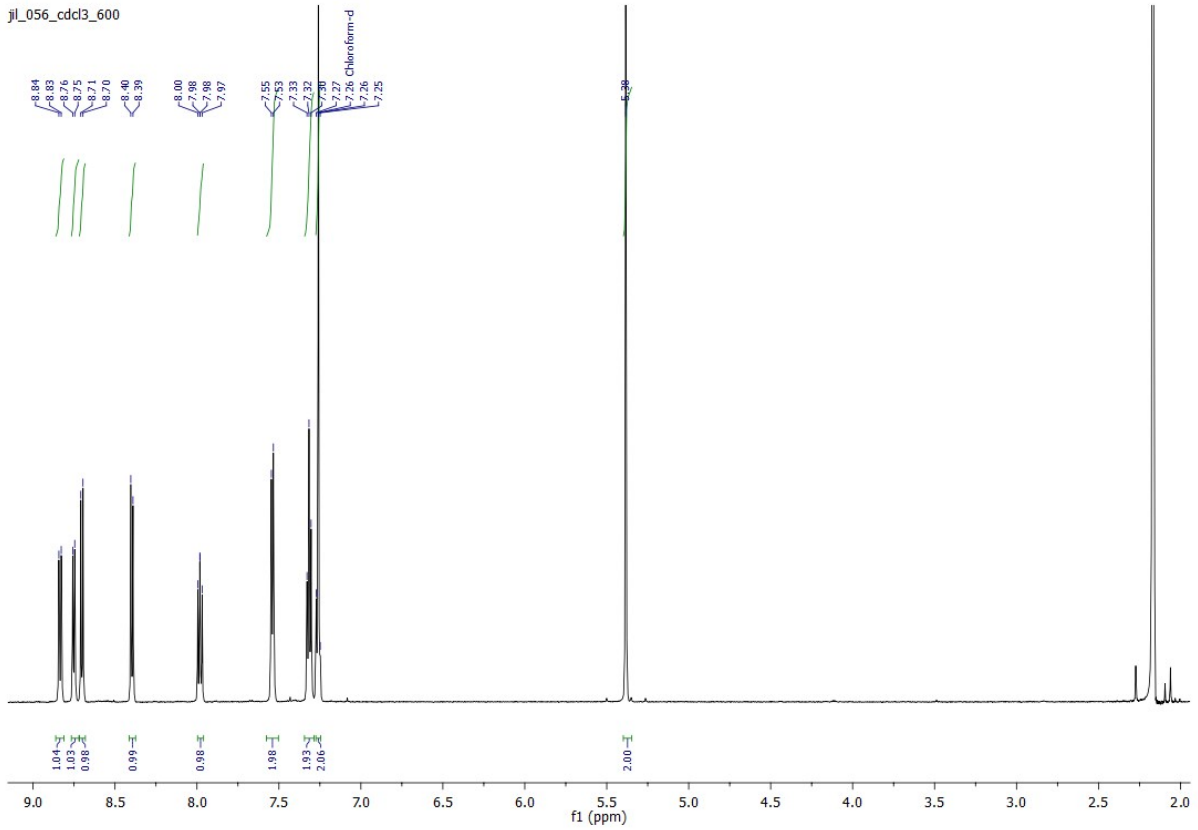

Fig. S79: *[1]H NMR spectrum of **L2a***

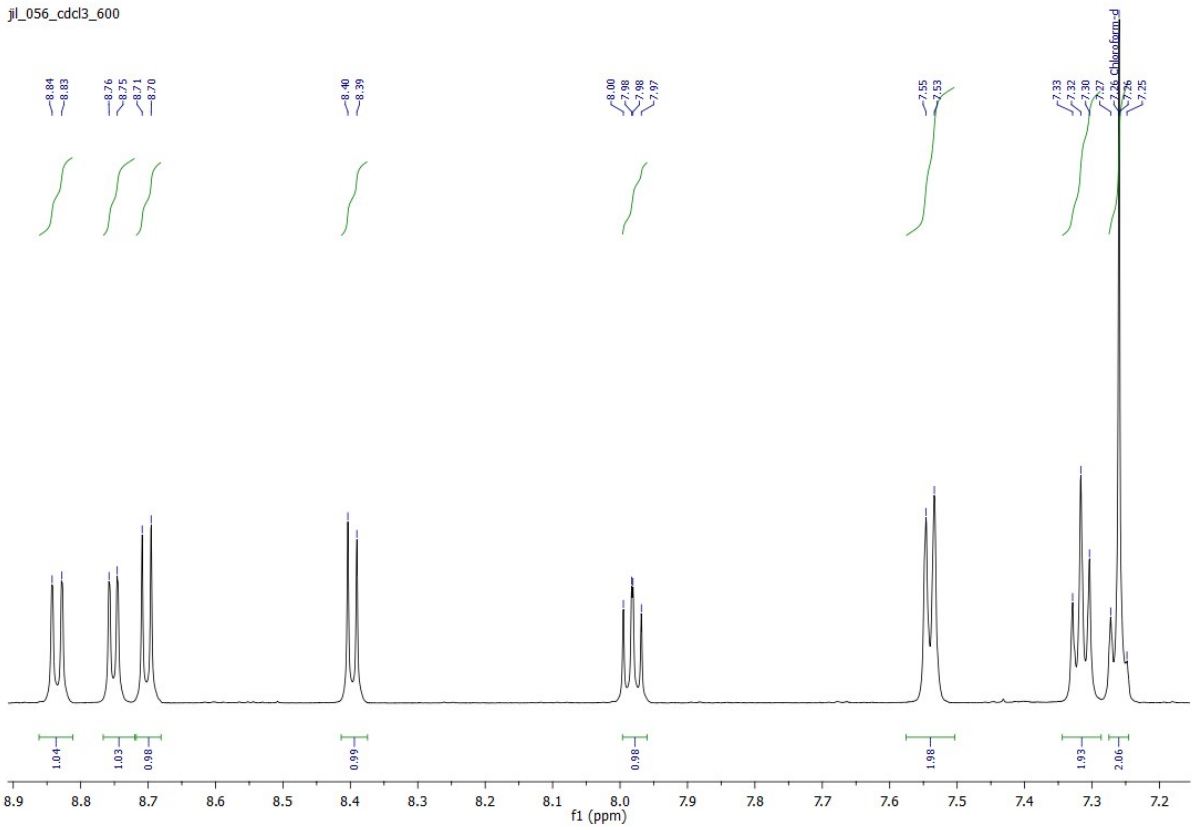

Fig. S80: *[1]H NMR spectrum with expanded aromatic region for **L2a.***

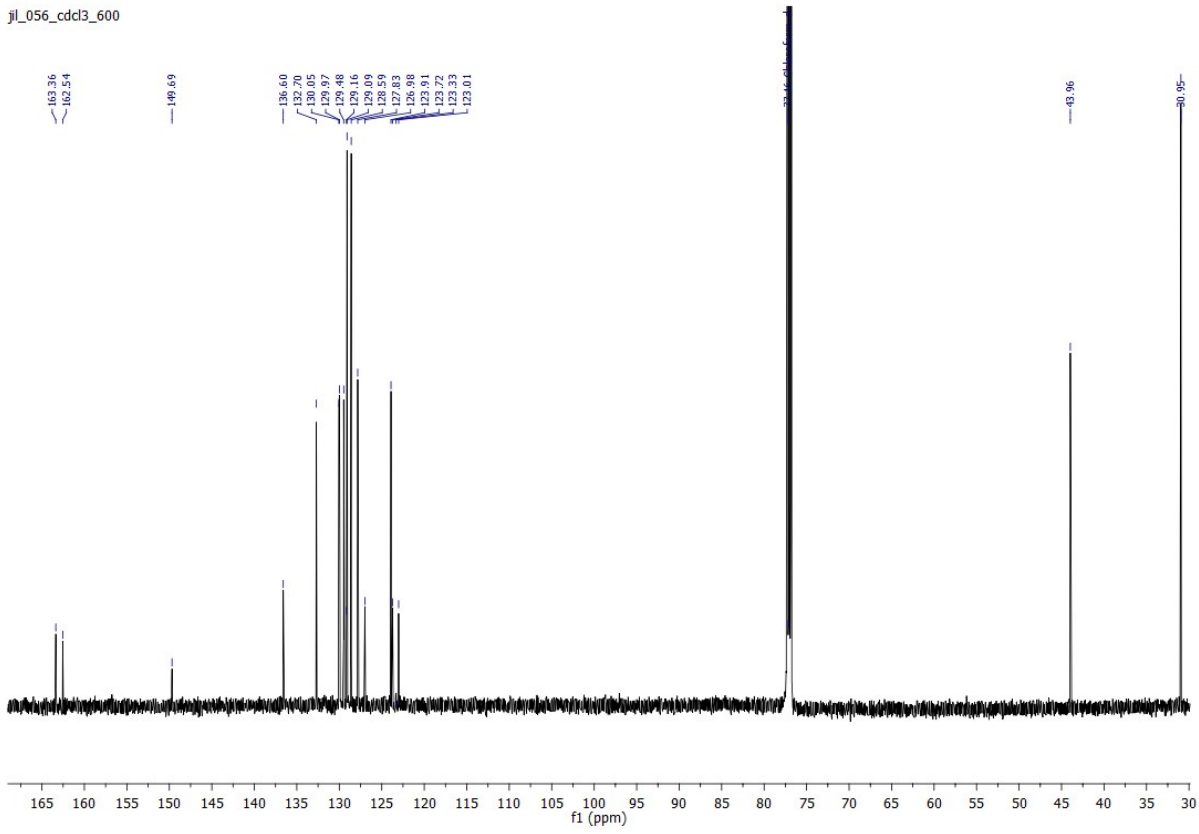

Fig. S81: *[13]C NMR spectrum for **L2a***

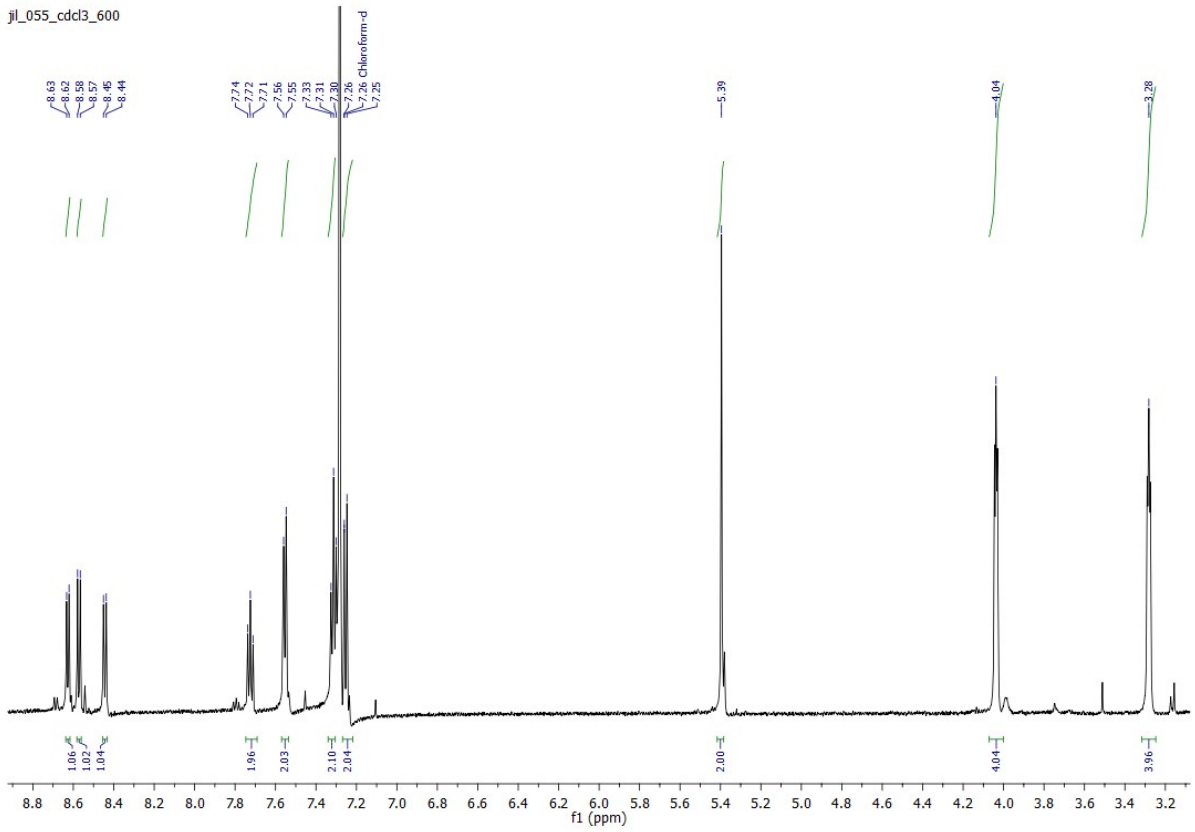

Fig. S82: *^{1}H NMR spectrum of **L2***

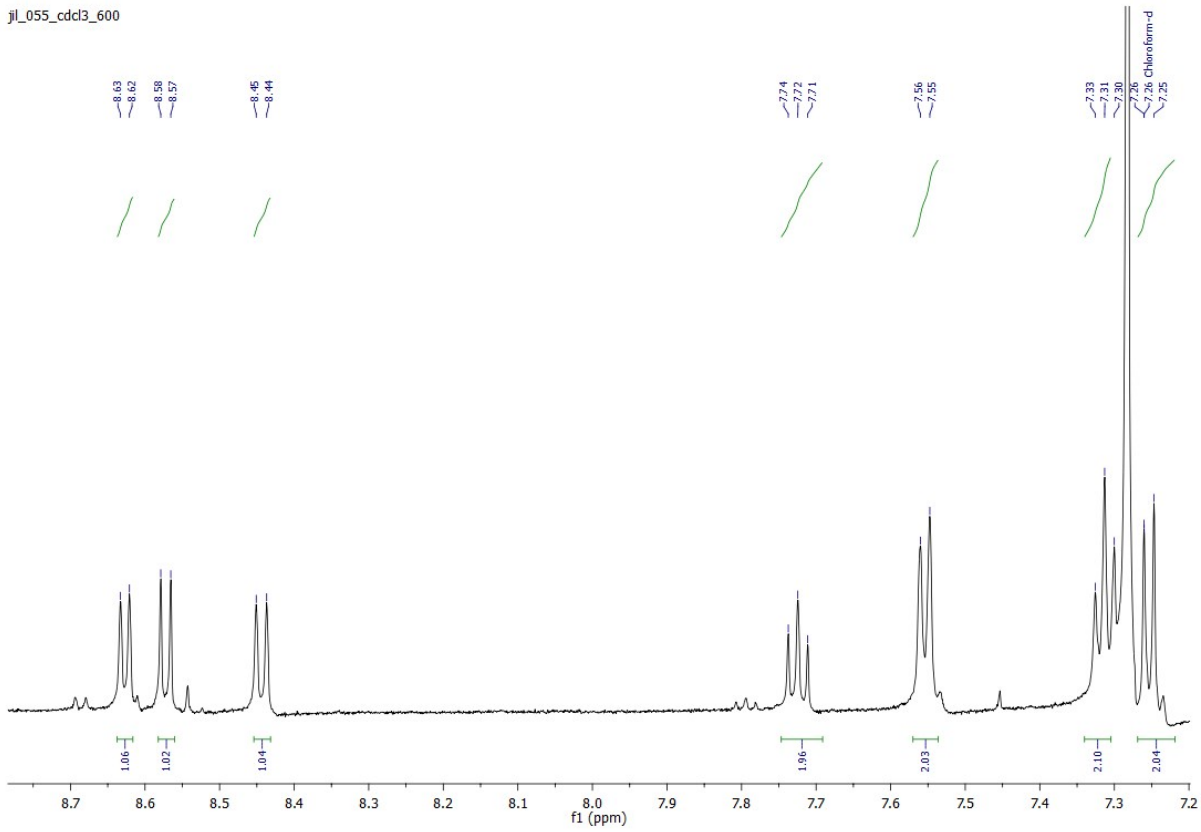

Fig. S83: *^{1}H NMR spectrum with expanded aromatic region for **L2.***

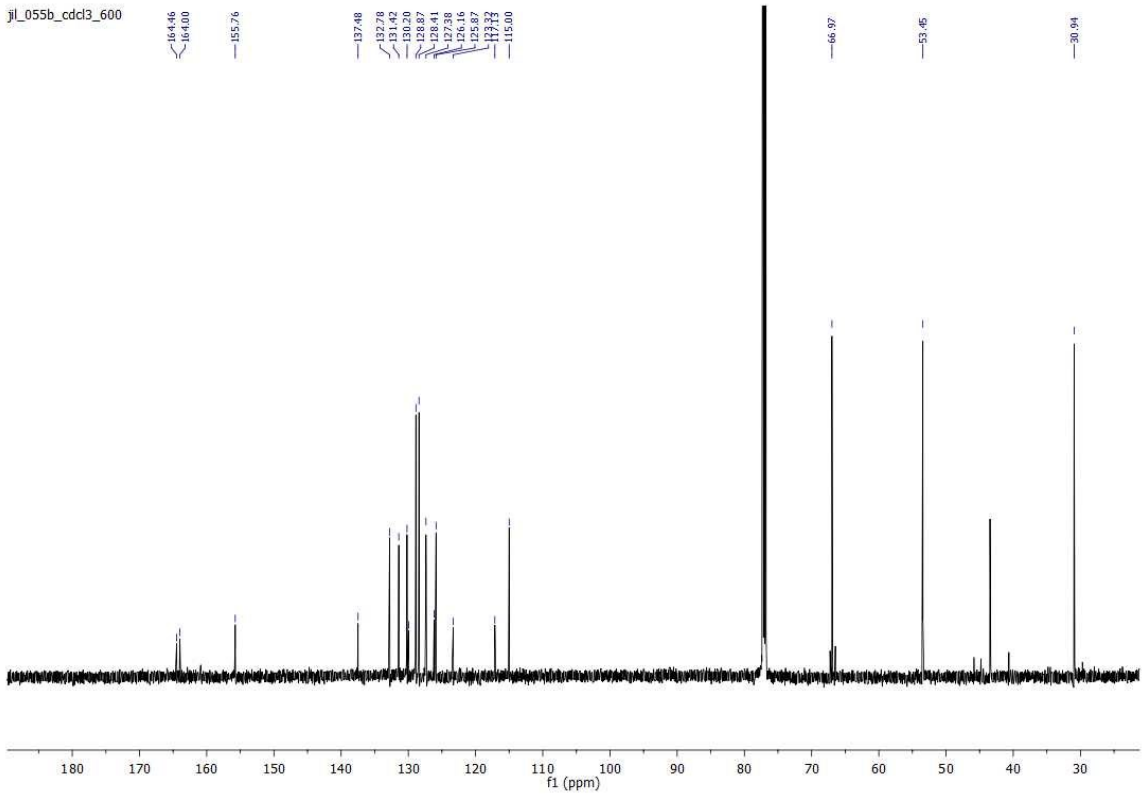

Fig. S84: *^{13}C NMR spectrum for **L2.***

References

S1. Bruker APEX-3, Bruker-AXS Inc., Madison, WI, 2016.

S2. SADABS, Bruker-AXS Inc., Madison, WI, 2016.

S3. G. M. Sheldrick, SHELXT - Integrated space-group and crystal-structure determination, Acta Crystallogr. Sect. A. 2015, 71, 3-8.

S4. G. M. Sheldrick, Crystal Structure Refinement with SHELXL, *Acta Crystallogr. Sect. C*. 2015, **71**, 3-8.

S5. J. I. Lovitt, C. S. Hawes, A. D. Lynes, B. Haffner, M. E. Möbius and T. Gunnlaugsson, Coordination chemistry of N-picolyl-1,8-naphthalimides: colourful low molecular weight metallo-gelators and unique chelation behaviours, *Inorg. Chem. Frontiers*, 2017, **4**, 296-308.

S6. *CrystalExplorer Version 3.1,* S.K. Wolff, D.J. Grimwood, J.J. McKinnon, M.J. Turner, D. Jayatilaka, M.A. Spackman, University of Western Australia, 2012.

S7. M.A. Spackman and D. Jayatilaka, Hirshfeld Surface Analysis, *CrystEngComm* 2009, **11** ,19-32.

S8. S. P. Kelley, A. Narita, J. D. Holbrey, K. D. Green, W. M. Reichert, R. D. Rodgers, Understanding the Effects of Ionicity in Salts, Solvates, Co-Crystals, Ionic Co-Crystals, and Ionic Liquids, Rather than Nomenclature, Is Critical to Understanding Their Behavior, *Cryst. Growth. Des*. 2013, **13**, 965-975.

S9. M. J. O'Neil, The Merck Index: An Encyclopedia of Chemicals, Drugs and Biologicals., Merck, 2000, New Jersey, 11th edn., 2000.

S10. N. Mataga, Y. Kaifu and M. Koizumi, Solvent Effects upon Fluorescence Spectra and the Dipole moments of Excited Molecules*, Bull. Chem. Soc. Jpn.*, 1956, **29**, 465-470.

S11. J. R. Lacowicz, *Principles of Fluorescence Spectroscopy,* Springer, New York, U.S.A., 2006.